Travail de fin d'études: Characterization of the spatial distribution of deposition in a small agricultural catchment. Comparison of a modeling approach using WaTEM/SEDEM with remote-sensing techniques (difference of DEMs)

Auteur : Bonaventure, Noémie
Promoteur(s) : Degré, Aurore; Baert, Pierre
Faculté : Gembloux Agro-Bio Tech (GxABT)
Diplôme : Master en bioingénieur : sciences et technologies de l'environnement, à finalité spécialisée
Année académique : 2022-2023
URI/URL : http://hdl.handle.net/2268.2/17713

LIÈGE université
Gembloux
Agro-Bio Tech

Characterization of the spatial distribution of deposition in a small agricultural catchment. Comparison of a modeling approach using WATEM/SEDEM with remote-sensing techniques (difference of DEMs).

Noémie Bonaventure

travail de fin d'etudes presente en vue de l'obtention du diplome de master bioingenieur en sciences et technologies de l'environnement

Annee academique 2022-2023

Co-Promoteurs: Aurore Degré et Pierre Baert

LIÈGE université
Gembloux
Agro-Bio Tech

Characterization of the spatial distribution of deposition in a small agricultural catchment. Comparison of a modeling approach using WATEM/SEDEM with remote-sensing techniques (difference of DEMs).

Noémie Bonaventure

travail de fin d'etudes presente en vue de l'obtention du diplome de master bioingenieur en sciences et technologies de l'environnement

Annee academique 2022-2023

Co-Promoteurs: Aurore Degré et Pierre Baert

Remerciements

Tout d'abord, je tiens à remercier mes promoteurs, Prof. Aurore Degré et Pierre Baert pour tous les conseils et commentaires constructifs qu'ils m'ont apporté tout au long de ce travail.

Merci également à Gilles Swerts pour toutes les précieuses informations sur le bassin versant de Chastre ainsi que pour la visite de terrain très instructive.

Je remercie également Prof. Jeroen Meersmans pour ses précieux conseils concernant l'analyse statistique.

Merci aux membres du jury d'avoir accepté d'en faire partie et pour la considération accordée à ce travail.

Merci à l'équipe du *Topo* pour leur accueil pendant ces quelques mois, et plus particulièrement à Anne-K, Manu, Matthieu et Benjamin.

Un grand merci à mes camarades de bureau de l'*Hydrotech*, Lisa, Margarita, Emilien, Lucie, Emilie et ceux qui sont passés nous voir pour les moments partagés ensemble en travaillant et pendant les pauses. Ma motivation à venir travailler tous les matins a grandement été influencée par la bonne ambiance du bureau.

Merci à ma famille, mes parents, mon frère et ma soeur pour leur soutien et plus particulièrement à mes parents pour leur aide dans la relecture. Merci aussi à Vegas, mon chien, pour toutes les balades bien utiles pour décompresser.

Enfin, puisque ce travail marque la fin de mes études dans cette belle faculté de Gembloux Agro-Bio Tech, je remercie tous les professeurs et assistants qui ont contribué à ma formation. Je remercie aussi mes ami·e·s étudiant·e·s avec qui j'ai partagé cinq merveilleuses années.

Résumé

La nouvelle Politique Agricole Commune (PAC) impliquant une nouvelle définition de la sensibilité des parcelles à l'érosion a ravivé les débats entre scientifiques, agriculteurs et décideurs politiques. Différentes méthodes et modèles existent pour étudier l'érosion, mais la communauté scientifique déplore un manque de données permettant de mesurer la distribution spatiale de ce phénomène. Cette étude se focalise sur un bassin versant agricole de Belgique centrale en région limoneuse. Le modèle WaTEM/SEDEM (WS) permettant de modéliser l'érosion et la déposition à l'échelle d'un bassin versant est comparé à l'approche par différence de modèles numériques d'altitudes (MNA). Dans cette méthode, deux MNA acquis à des périodes différentes sont soustraits l'un à l'autre pour identifier les zones de déposition (différence positive) et d'érosion (différence négative). Différentes sources de données de MNA ont été exploitées : Modèle Numérique de Terrain (MNT) et Modèle Numérique de Surface (MNS) Lidar et photogrammétriques, sur une échelle temporelle d'une décennie. Les résultats montrent que la déposition modélisée avec WS se concentre dans les axes d'écoulement concentré (thalwegs). Les MNT Lidar, qui semblent les plus fiables pour étudier ce phénomène, confirment cette tendance, avec une proportion de déposition supérieure de 40% dans les thalwegs par rapport aux versants. En parallèle, les cartes de différences de MNA sont employées dans une analyse statistique visant à identifier les variables influençant la répartition spatiale de l'érosion et de la déposition. Les résultats montrent qu'il est possible de prédire les différences d'altitude sur base d'un modèle dont les variables explicatives impliquent des variables topographiques, climatiques et de pratiques agricoles. L'utilisation de MNT et MNS, sous réserve d'une prise en compte de l'imprécision associée ainsi que de l'influence de la végétation pour les MNS, montre des résultats encourageants dans leur exploitabilité pour étudier l'érosion sur une décennie.

Abstract

The new Common Agricultural Policy (CAP) has led to a new definition of the fields sensitivity to soil erosion. It revived the debates between scientists, farmers, and policy makers. Different methods and models exist to study erosion, but soil scientists point out a lack of data to study the spatial distribution of this phenomenon. This study focuses on an agricultural catchment of central Belgium in the Loess belt. We compared the model WaTEM/SEDEM (WS) enabling to model the spatial distribution of erosion and deposition at a catchment level to the difference of Digital Elevation Model (DEM) method. In this method, two DEMs, acquired at different periods, are subtracted from each other to spot the zones experiencing deposition (positive difference) and the eroded zones (negative difference). Different DEM data sources are exploited: Digital Terrain Model (DTM), Digital Surface Model (DSM), from Lidar and photogrammetry on a temporal scale of one decade. The results show that deposition modeled with WS is concentrated in the rills. The lidar DTMs, which seem the most reliable to study this phenomenon confirm this tendency, with a proportion of deposition 40% higher in the rills than in the inter-rills. In parallel, we carried out a statistical analysis of the maps of DEM differences to identify the variables influencing the spatial distribution of erosion and deposition. Our results show that it is possible to predict the elevation differences based on a model including variables that involve topography, climate and agricultural practices. Taking into account the uncertainty and the influence of vegetation, DTM and DSM show encouraging results in their usability to study erosion over one decade.

Contents

List of Figures

List of Tables

Acronyms

CAP Common Agricultural Policy. 2

DEM Digital Elevation Model. 4, 12

DoD Difference of DEM. 4, 7

DSM Digital Surface Model. 12

DTM Digital Terrain Model. 12

FCR Facies, Crop cover, Roughness. 12

GAEC Good Agricultural and Environmental Conditions. 2

IQR Interquartile Range. 18

MLR Multiple Linear Regression. 18

PCA Principal Components Analysis. 18

RUSLE Revised Universal Soil Loss Equation. 5

UAV Unmanned Aerial Vehicle. 12

USLE Universal Soil Loss Equation. 5

Chapter 1

Introduction

1.1 Context

Erosion is a topic of major concern in the agricultural sphere nowadays. The Common Agricultural Policy (CAP) for 2023-2027 entered into application on the 1st of January 2023 (European Commission, nd). It implies several changes in comparison with the previous CAP, especially on the conditionality principle Good Agricultural and Environmental Conditions (GAEC) which defines the *"minimum land management reflecting site-specific conditions to limit erosion"*(European Commission, 2015). In Belgium and more specifically in Wallonia, this results, among others, in a new classification of erosion risk at the parcel level which is not always received positively by the farmers (Rotili, 2023). The previous methodology to determine the erosion risk, called "R10/R15" was only based on the fact that the parcel presents more than 50 ares or 50% of its area with a slope higher or equal to 10% (R10) or 15% (R15). The new methodology relies on the soil sensibility to erosion (based on the texture and organic matter content), the topography (slope gradient and slope length), and the rainfall aggressivity (erosivity) (SPW, 2023). In order to realize why this is so important, it is essential to understand the process of erosion and the negative impacts associated. Indeed, the better this process will be understood, the better the side-effects can be avoided through an appropriate management of the agricultural soils.

1.2 What is soil erosion

Soil erosion is a process that involves the detachment of soil particles, their transport and their deposition elsewhere. Different agents can be responsible for the detachment: water, wind, agricultural practices, gravity, glaciers, and crop harvesting. Erosion can cause an alteration of the soil surface and modify the relief (Dautrebande et al., 2006).

In Belgium and more specifically in Wallonia, the main types of erosion occurring in agricultural soil are erosion caused by water, tillage and soil loss due to harvesting. Some landslides can also happen (Dautrebande et al., 2006). Erosion can cause different problems occurring on- and off-site, which are likely to lead to important costs.

- **On-site effects**: Those problems are particularly important in agricultural land and include the reduction of cultivable soil depth and the decline in soil fertility. Both problems result from the redistribution of soil particles within the field and the loss of soil from the field, the breakdown of soil structure and the decline in organic matter and nutrients. The loss of soil productivity can lead to an increase in fertilizer use and ultimately to the abandonment of land for agriculture. This can have consequences on food production and

food security and can decrease the value of land.

- **Off-site effects**: Those effects occur downstream in the catchment, or downwind and result from sedimentation. The accumulation of sediments in rivers, canals, drainage ditches or reservoirs can enhance the risk of flooding by reducing their transport or storage capacity. It can also shorten the design life of hydroelectric and irrigation systems. Moreover, chemicals such as nitrogen and phosphorous can be adsorbed to sediments, which can ultimately cause eutrophication of the surface water bodies once the sediments are transferred to them. Another consequence of erosion is the release of CO_2 to the atmosphere, which makes it a contributor to climate change. Indeed, erosion causes the breakdown of soil aggregates into primary particles of clay, silt and sand. The soil organic carbon held on clays is therefore oxidized and released in the atmosphere in the form of CO_2 (Morgan, 2005).

Originally, soil erosion is a natural process but it has been increased over the last decades due to modification of the drivers through human activities. Indeed, human activities are likely to influence the first three factors of erosion, identified as: *"(i) erosivity of the erosive agent or its capacity to detach and transport soil particles; (ii) erodibility of the soil or the inverse of the soil's resistance against the detachment and transport of its particles; (iii) plant and litter cover; and (iv) slope of the terrain"* (Morgan, 2005). This will be illustrated by several examples. We can distinguish the external drivers (rainfall) that are indirectly affected by human activities through climate change, and the drivers directly affected by human activities. Climate change scenarios expect an increase in rainfall erosivity especially in the Mediterranean climate regions with more intense rainfalls in autumn (Stolte et al., 2016). In Belgium, the precipitation intensity is also expected to increase. In the most pessimistic scenario (RCP 8.5), both the number of days with at least 10 mm of rainfall and the 99^{th} centile of daily precipitations - two indices used to describe extreme rainfalls - increase by 2100 (IRM, 2020). Agricultural practices have a direct impact on the drivers. Ploughing can enhance the erosivity of the surface runoff and enhance soil erodibilty by destroying soil aggregates and reducing the formation of new aggregates due to a reduction of soil organic matter content. The use of heavy machinery in agricultural fields is likely to cause compaction of the topsoil which reduces the infiltration capacity. The density of vegetation is often reduced in croplands in comparison with natural vegetation. The soil surface is therefore less protected against rainsplash and has less resistance to overland flow (Stolte et al., 2016). Finally, even if the slope of the terrain is not affected by humans, the slope length of the parcel can be modified by grouping different parcels together into longer ones. This phenomenon was widely observed in Belgium since the last century and can increase the risk of erosion at a parcel level when the parcel length is increased in the slope direction (Dautrebande et al., 2006).

The main problem of erosion is that the rate at which this phenomenon occurs currently is higher than the pedogenesis rate. Verheijen et al. (2009) defined the concept of tolerable soil erosion as: *"any actual soil erosion rate at which a deterioration or loss of one or more soil functions does not occur"*, with actual soil erosion meaning *"the cumulative amount of soil lost by all recognized erosion types"*. They estimated that the current tolerable erosion rates in Europe range from ca. 0.3 to 1.4 $t.ha^{-1}.yr^{-1}$ (corresponding to soil formation rates), while the actual soil erosion rates vary between 3 and 40 $t.ha^{-1}.yr^{-1}$. Particularly, they noted that soil erosion rates only appear to exceed tolerable rates in cultivated soils or in soils affected by other human disturbances. Tilled arable soils seem to experience an important difference between soil formation and erosion rates, with reported erosion rate ranges being many times greater than reported soil formation rate ranges.

1.3 Methods used to quantify erosion

Different methods exist to estimate erosion. Each of those methods has its own advantages and side-effects and associated costs that need to be taken into consideration when selecting the method to undertake in the case of the study.

A common data measured in erosion studies is the runoff and sediment export at the catchment outlet. In those cases, the outlet is equipped with a flume, a flowmeter and a sampler to measure the water flow and the suspended sediment concentration (Van Oost et al., 2005a; Cantreul et al., 2020). Nevertheless, even if this approach enables to calibrate or validate erosion models, it does not give any information about the spatial distribution of erosion and deposition (Van Oost et al., 2005a).

Plot studies use bounded or unbounded plots of a fixed size to measure runoff produced from rainfall events. Those can be either simulated by using rainfall simulators or monitored from natural precipitations (Parsons, 2019). This method has been largely used in the United States of America for the development of the Universal Soil Loss Equation (Wischmeier & Smith, 1978).

Field surveys and monitoring are other approaches that can be used to estimate erosion in fields or small catchments. During field surveys, experts identify rills and gullies and estimate their volume (Parsons, 2019). Van Oost et al. (2005a) converted the volumetric estimation of rills and gullies into erosion rates with a constant bulk density. They also identified the deposits and measured the sediment thickness. Then, they converted the sediment volumes into deposition rates with the value of the bulk density of the deposits. The monitoring can also concern the land use, soil surface roughness, soil surface crusting stage, crop cover, which might be useful input data in the models.

For a long-term erosion study, diachronic soil surveys that rely on the comparison of an historic soil map with more recent observations might be an option to consider. They enable to show trends in the evolution of the soil profiles properties in the landscape, by spatializing the erosion and deposition processes, but very accurate quantifications are impossible (Pineux et al., 2017b).

Another option investigated to measure erosion is the measurement of change in the soil surface level. Erosion pins are among the most widely used methods to do so. Those consist of pins made out of iron, wood, or any other cheap and readily available material that is not likely to rot or decay. The pins are distributed in the study area and driven into the soil to a certain depth. The top of the pin that is above the surface is measured and serves as the reference measurement. After a certain period, the new pin height is measured and changes in the soil surface can be determined by comparing the two measures (Hudson, 1993).

Another similar approach concerns the use of graduated rulers. Those rulers are placed in the fields at chosen locations and the erosion or deposition is measured after a certain amount of time (Cantreul et al., 2020). With graduated rulers the principle is the same as with erosion pins, but the height above the soil surface can be read directly on the ruler.

The development of remote sensing techniques has improved recently. It is therefore now possible to acquire more and more precise Digital Elevation Models (DEMs) (Lisein et al., 2017). The spatial distribution of erosion and deposition can be estimated by computing the difference of 2 DEMs acquired at different time intervals. The change in elevation between the 2 DEMs is computed as $\delta E = Z_2 - Z_1$ where Z_2 refers to the more recent DEM and Z_1 to the oldest one. In the DEM of Difference (DoD), negative and positive values show respectively erosion and deposition (Williams, 2012). Nevertheless, an important condition to the use of this method is that the DEMs have to be taken at the same period in the crop rotation (Pineux et al., 2017a).

Tracing is a different approach that consists in using natural and fallout radionuclides to study soil erosion. The most widely used radionuclides are ^{137}Cs, ^{210}Pb and ^{7}Be (Parsons, 2019). ^{137}Cs is a globally distributed fallout radionuclide that comes from nuclear weapons testing in the 1960s and from the power plant accident of Chernobyl in 1986. However, several authors consider that due to its short half-life (30.17 years) and the inhomogeneous spatial distribution of the fallout in Central and Western Europe caused by the Chernobyl accident, its use as an erosion tracer is limited. Therefore, some suggest using other radionuclides such as $^{239+240}Pu$ and ^{10}Be that are respectively suitable for short (decadal) and long (millennial) -term erosion rates estimations (Loba et al., 2021). The principle of this method is to measure the concentration of the radionuclide considered in a location where the soil is assumed to be undisturbed (upper parts of slopes) and to compare the radionuclide concentration at different locations. For example, Zhidkin et al. (2023) estimated soil erosion with ^{137}Cs and computed the annual rate of soil erosion as :

$$A = (Z_n - Z_0) \times \rho \times 25 \times 100/(Z_0 \times T) \tag{1.1}$$

with: A: the annual rate of soil erosion (negative value) or sediment accumulation (positive value) ($t.ha^{-1}.yr^{-1}$); Z_n: the ^{137}Cs reserve in the sampling point (kBq/m^2); Z_0: the initial Chernobyl derived ^{137}Cs fallout (kBq/m^2); ρ: soil bulk density (g/cm^3); T: the duration of the estimated period (30 years from the moment of the Chernobyl accident to the sampling); 25: the depth of soil sampling; 100: unit conversion factor. This method relies on several assumptions about the tracers: *(a)* Uniform local fallout distribution. *(b)* ^{137}Cs fallout is rapidly adsorbed onto soil particles. *(c)* Subsequent redistribution of ^{137}Cs reflects sediment movement. *(d)* Estimates of rates of soil loss can be derived from measurements of soil ^{137}Cs inventories (Walling & Quine, 1992).

1.4 Modeling erosion

Models are widely used to estimate and represent erosion in a wide range of conditions (Morgan, 2005). The most famous model is the USLE equation (Universal Soil Loss Equation) (Wischmeier & Smith, 1978). This empirical model is meant to compute the diffuse erosion, with as basis equation:

$$A = R \times K \times LS \times C \times P \tag{1.2}$$

where: A: annual average soil erosion ($Mg.ha^{-1}.yr^{-1}$), R: rainfall-runoff erosivity factor ($MJ.mm.h^{-1}.yr^{-1}$), K: soil erodibility factor ($Mg.h.MJ^{-1}.mm^{-1}$), LS: slope length and steepness factor (dimensionless), C: land cover and management factor (dimensionless), P: soil conservation or prevention practices factor (dimensionless). The RUSLE (Revised Universal Soil Loss Equation) is an adaptation of this model (Renard et al., 1997).

The model that we use in this study is the WaTEM/SEDEM (WS) model. It is a spatially distributed soil loss and sediment delivery model based on the RUSLE equation. It is divided into two modules, where WaTEM (Water and Tillage Erosion Model) concerns water and tillage erosion (Van Oost et al., 2000) and SEDEM (SEdiment DElivery Model) refers to sediment transport and sedimentation (Van Rompey et al., 2001). A complete description of the model can be found in the WaTEM/SEDEM Manual (Notebaert et al., 2006). In the WaTEM module, the RUSLE equation is adapted to a two-dimensional landscape by using the unit contributing area instead of the slope length in the computation of the slope length factor (L). The principle of the water erosion model is to consider the erosion rate (E_{PTot}) as the sum of the potential

for rill (E_{PR}) and inter-rill erosion (E_{PIR}) (equation 1.3).

$$E_{PTot} = E_{PR} + E_{PIR} = R \times K \times L \times S \times C \times P \tag{1.3}$$

For each cell, the sediment inflow and the sediment of the cell is compared to the transport capacity (equation 1.4). If the sediment inflow is higher than the transport capacity, deposition occurs.

$$T_C = k_{TC} \times E_{PR} \tag{1.4}$$

The amount of sediment leaving the cell is then equal to the transport capacity. Then, the potential inter-rill erosion is computed as:

$$E_{PIR} = a \times R \times K \times S_{IR} \times C \tag{1.5}$$

where

$$S_{IR} = 5.0 \times Sg^{0.8} \tag{1.6}$$

and a is a coefficient. Sg is the slope gradient (m/m)

The tillage erosion, which is due to variations in tillage translocation over a landscape is controlled by the change in the slope gradient. In convexities, erosion happens while accumulation takes place in concavities. First, the net downslope flux due to tillage translocation (Q) is computed as:

$$Q = k_{til} \times S = -k_{til} \times \frac{dh}{dx} \tag{1.7}$$

with k_{til}, the tillage transport coefficient, and S the slope gradient. Then, the local erosion or deposition rate (E_t) is calculated as:

$$E_t = \rho_b \times \frac{dh}{dt} = -\frac{dQ}{dx} = k_{til} \times \frac{d^2h}{d^2x} \tag{1.8}$$

1.5 Problematic and hypothesis

One of the main problems faced by scientists to study erosion is the lack of spatially distributed data, which are essential to calibrate and validate spatially distributed models (Batista et al., 2019). Jetten et al. (2003) pointed out the fact that only a few studies compare the predicted erosion patterns to the observed ones, while the majority of the model tests and sensitivity analyses focus on outlet-based data only.

More particularly in the case of the use of the WaTEM/SEDEM model, some authors report a lack of representativity in the spatial distribution of deposition in the catchment (Zhidkin et al., 2023). Indeed, the output of the model shows deposition mainly in the valley bottom or in the rills, while in reality, some landscape features such as field boundaries, grass strips, or other topographic and soil properties parameters are likely to influence the deposition rate. This "problem" is in fact inherent to the way the model is constructed. Based on the equations presented before (1.3-1.8), it appears that the deposition has 2 possible sources. It can either be due to the tillage erosion (1.7,1.8) or to the water erosion (1.3-1.6). Between those two components, only the water erosion is divided into inter-rill and rill erosion. Therefore, this is the one that should be more investigated to understand why the model has the tendency to show less deposition in the inter-rills. In this component, the deposition is controlled by the value of T_c, the transport capacity. If we combine the equations, we obtain for a bare soil and without particular soil conservation practices ($C = 1$ and $P = 1$):

$$T_C = k_{tc} \times (E_{PT} - E_{PIR}) = R \times K \times k_{TC} \times (LS - aS_{IR}) \tag{1.9}$$

Here, it is important to understand all the parameters of the equation. The only one that has not been explained yet is k_{TC}, which is the transport capacity coefficient (in m). It *"describes the proportionality between the potential for rill erosion and the transport capacity. It can be interpreted as the theoretical upslope distance that is needed to produce enough sediment to reach the transport capacity at the grid cell, assuming a uniform slope and discharge"* (Van Rompey et al., 2001). This coefficient needs to be calibrated and validated before its use in the model. The hypothesis of this study is that this coefficient is not uniform in the catchment and the aim will be to determine which variables may influence its value. All in all, it is clear that the topographic variables play an important role in the spatial distribution of deposition modeling in WaTEM/SEDEM. In more recent studies, other parameters such as tillage direction are tested to determine their influence on erosion and deposition in the inter-rills in agricultural catchments.

Therefore, the aim of this study is to test whether deposition can actually occur in the inter-rills. Moreover, the parameters that influence erosion and deposition will be determined.

The estimation of erosion and deposition will be made by using the Difference of DEM approach. This method has already been used in this specific catchment and has shown encouraging results, even if it faced technical issues related to ground control points (Pineux et al., 2017a).

A particularity of this study relies on the scale at which it is conducted. In terms of spatial scale, the study area is a small agricultural catchment. This is different from most approaches that focus either on the field scale or on large catchments. The temporal scale is of around 10 years. It is therefore neither an event-based approach nor a long-term study, which are the most common scales used in erosion studies.

Chapter 2

Materials and methods

2.1 Study area

The study area is a small agricultural catchment of 124 ha located in Chastre, in the province of Walloon Brabant, in the Belgian loess belt (figure 2.1). The coordinates of the outlet are 50°36'23.111"N, 4°35'42.542"E. The catchment is dominated by agricultural areas (98%). The elevation varies between 128 and 161 m and the slope ranges from 0 to 9%. A complete description of the catchment can be found in Pineux et al. (2017a) and Cantreul et al. (2020).

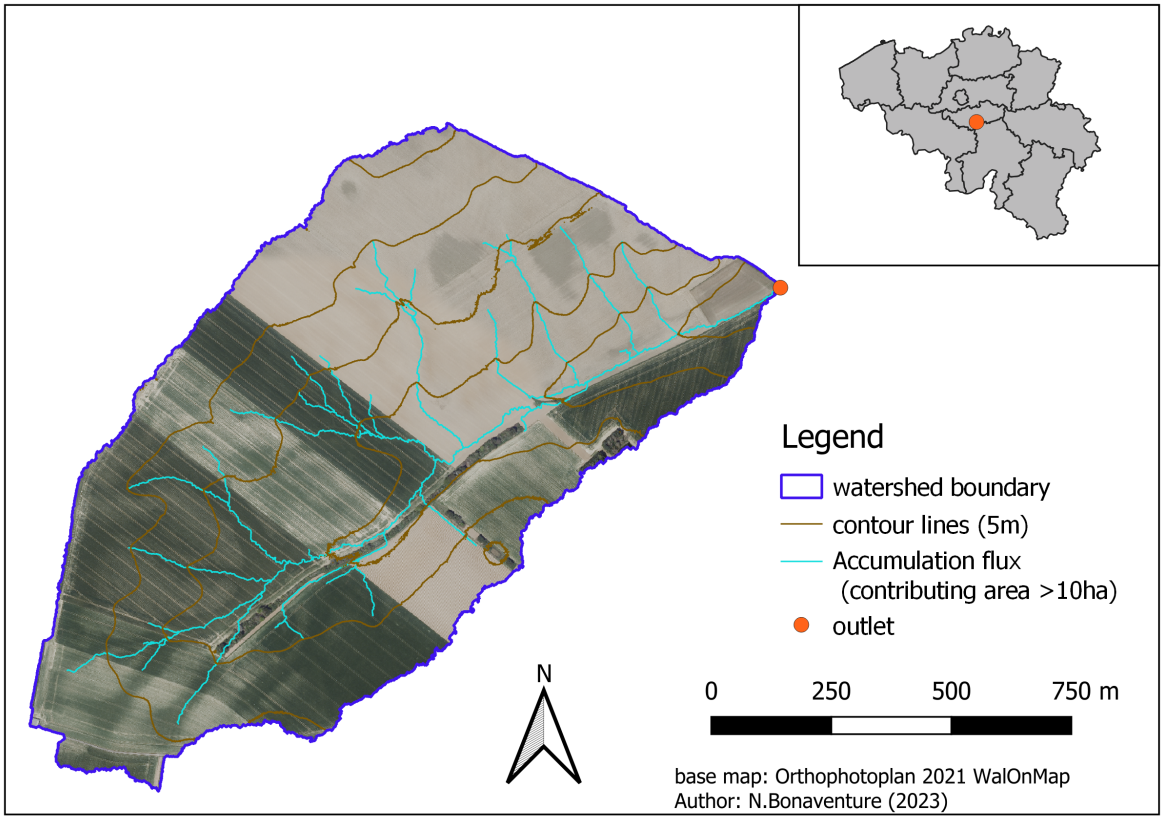

Figure 2.1: Catchment presentation and location

The catchment is divided into 12 main parcels, which are sometimes subdivided into smaller ones depending on the annual cultural plan. The crop rotation consists in mainly sugar beat

(*Beta vulgaris*), winter wheat (*Triticum aestivum*), potatoes (*Solanum tuberosum*), maize (*Zea mays*), chicory (*Cichorium intybus*), and barley (*Hordeum vulgare*). Linen (*Linum usitatissimum*) and rapeseed (*Brassica napus*) can also be found. The complete representation of the parcel division and the crop rotation is presented in figure 2.2. The parcels identified as n°12 are always planted with maize which is dedicated to wild fauna for hunting purposes. The map presenting the number of the parcels can be found in figure 2.8 in section 2.4.1.

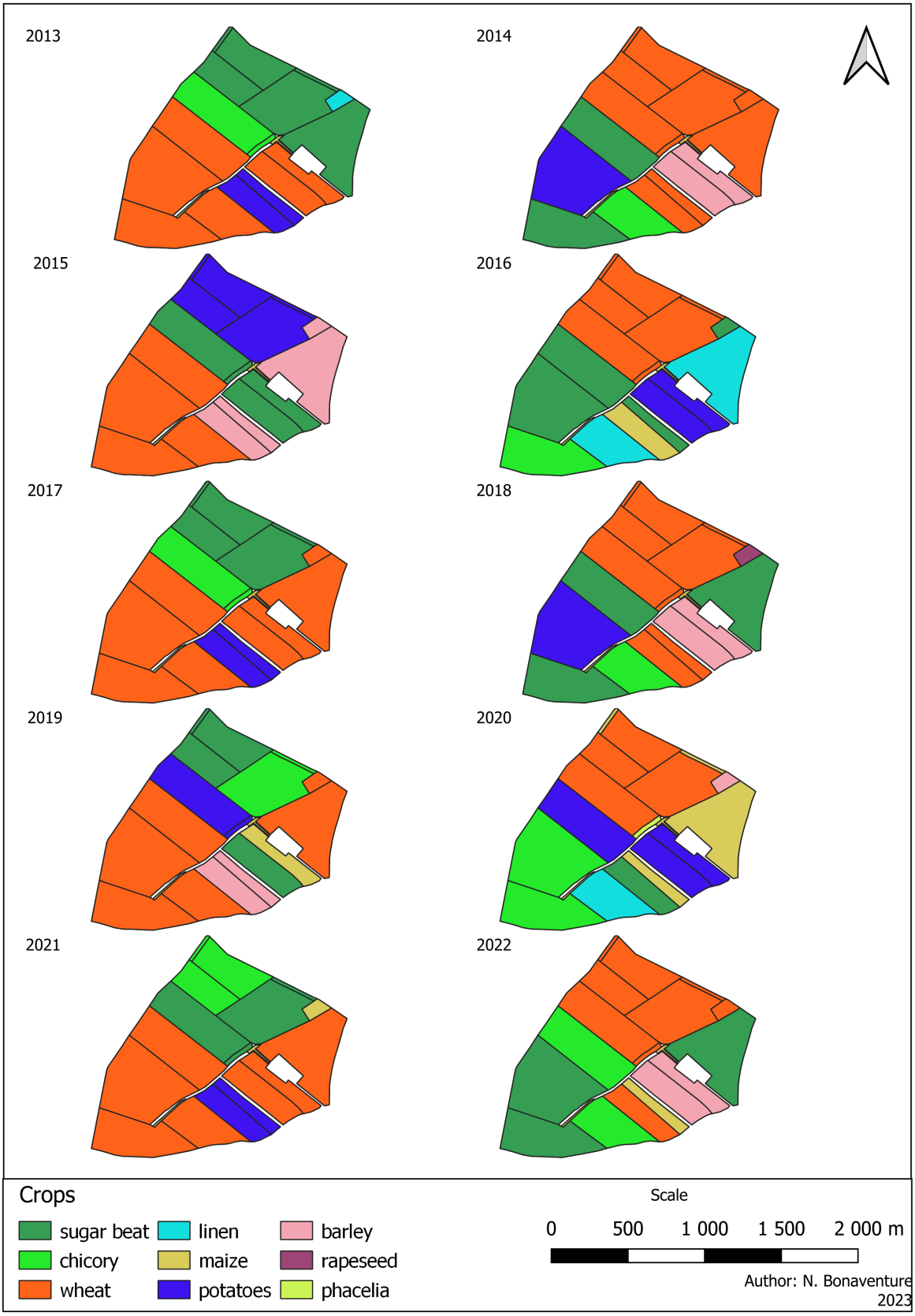

Figure 2.2: Crop rotation from 2013 to 2022

Over the past years, and especially in July 2021, some important rainfall events happened

in the catchment. This event caused the formation of gullies in the fields (figure 2.3). This is important to take into account because the farmer rearranged the soil in order to fill in the gullies. This was observed on the field (figure 2.4) and is also clearly visible on the orthophotoplan of 2022 provided on WalOnMap (`https://geoportail.wallonie.be`), as shown in figure 2.5.

Figure 2.3: Gullies observed in the fields (Gilles Swerts)

Figure 2.4: Observation of soil translocation on the field (Gilles Swerts)

Figure 2.5: Orthophotoplan WalOnMap 2022 showing the filling of gullies by the farmer

2.2 Available data

The catchment is equipped with several instruments such as a meteorological station that measures, among others, the precipitations on a 5min time step. In addition to this, field surveys are done every month to determine the FCR classification (Facies, Crop cover, Roughness), based on the methodology of Cerdan et al. (2001).

Every year since 2011, aerial surveys were carried out with drones, also called Unmanned Aerial Vehicles (UAVs) to produce DEMs of various resolutions by using photogrammetry. For this data source, it is important to distinguish between the Digital Terrain Model (DTM) and the Digital Surface Model (DSM). The latter takes into account the vegetation or buildings while for the first only the ground elevation is computed. This can have a large influence on the analysis. Most of the DEMs produced for the catchment using UAVs were DSM, except in 2022 for which a DTM was also produced. However, in order to avoid a too important influence of the vegetation, most of the DSMs were acquired during the winter.

Another source for the DEM is the "Service Public de Wallonie", through the WalOnMap geoportal (`https://geoportail.wallonie.be`). Again, there are 2 types of DEMs available (DTM and DSM). They were acquired in 2013-2014 (Lidar acquisitions: 12/12/2012 to 09/03/2014) and 2021-2022 (Lidar acquisitions from 19-02-2021 to 05-03-2022). An overview of all the DEMs available with the source, the flight dates and the resolution is presented in table 2.1.

Table 2.1: Source, date and resolution of DEMs available

Source (UAV/WalOnMap)	**Date**	**DTM/DSM**	**Resolution**
WalOnMap	2013-2014	DTM	1m
		DSM	
	2018	DSM	
	2021-2022	DTM	
		DSM	
		DTM	0.5m
		DSM	
UAV	11-12-12	DSM	∼0.12m
	12-12-13		∼0.12m
	23-05-14		∼0.12m
	??-12-15		∼0.15m
	13-12-16		∼0.12m
	13-03-17		∼0.25m
	06-02-18		∼0.3m
	14-02-19		∼0.3m
	17-03-20		?*
	21-04-22	DTM	0.5m
		DSM	0.018m

*No DSM was found

2.3 DEM analysis

2.3.1 Influence of the vegetation

Prior to the difference of DEMs and the statistical analysis, an investigation of the data quality is necessary. More precisely, since there are different DEM types (DSM and DTM), it is essential to determine which data source is the most relevant to use. To do so, a visual comparison based on transects in the catchment was carried out. The data provided on WalOnMap have the

advantage to be either DTM and DSM and can therefore be compared to see to what extent the vegetation influences the values.

2.3.2 Uncertainty analysis

For each DEM, some uncertainty is present, due to the precision of the measurement and building process of the DEM. It is important to make sure that the potential errors in the DEM due to precision remain lower than the changes that can be expected in the elevation. The precision in Z of the different DEMs can be found in table 2.2. Another verification approach consists in comparing different points in the catchment that are not supposed to encounter an elevation change over the years. Such points can be for example located on infrastructures such as buildings or roads. Since the catchment is mostly composed of agricultural fields, the only elements that can be used as "reference" are the road and the path around the catchment boundaries.

Table 2.2: Precision of DEMs

Data source	**Precision in z**
DSM 2013 (UAV)	around 0.04 m (Pineux et al., 2017)
DSM and DTM 2022 (UAV)	around 0.07 m
DSM and DTM WalOnMap	0.12 m on the whole Walloon territory (https://geoportail.wallonie.be)

2.3.3 Difference of DEM

As explained earlier, the difference of DEMs have 2 data sources: the DEMs produced by UAV flight data acquisition and the DEMs provided by WalOnMap. To make sure that the results can be compared, the time extent has to be similar. Therefore, since the available WalOnMap DEMs were collected in 2013-2014 and 2021-2022, the DEMs produced by UAVs that will be used are the ones of 2013 and 2022. The difference of DEM is always computed as:

$$\Delta DEM = DEM_{recent} - DEM_{old} \tag{2.1}$$

The resolution of the WalOnMap DEMs will be 1 m. This will serve as the reference for the DEMs produced with UAVs flights, which will be resampled to 1 m resolution (using the bilinear method). The projection system chosen for this study is the Belgian Lambert 72 (EPSG:31370).

2.3.4 Transects

In order to estimate in a more qualitative way the influence of the field boundaries, flow accumulation streams or transition features in the catchments, some transects were made across the catchment (figure A.11 in the appendix) to visualize the elevation changes related to erosion and deposition. The DEMs produced at different years were compared to determine if they can be used to observe the temporal evolution of erosion and deposition.

2.4 Statistical analysis

One of the objectives of this study is to determine which variables can influence the spatial distribution of erosion and deposition. To do so, a statistical analysis will be conducted. The variables are represented by different raster layers and the observations will be created by extracting the values of the raster layers for a certain number of points in the catchment area.

2.4.1 Variables tested

Based on the literature review, variables that may influence erosion were identified and for each variable, a raster layer was created.

- **Slope**
  The slope is an important topographic parameter influencing erosion and deposition. It was determined in QGIS based on the DEM of 2013-2014 provided on WalOnMap and expressed in percent.

- **Curvature**
  The slope curvature was determined with the "Slope, Aspect, Curvature" tool provided in the QGIS "SAGA" tools, with the "general curvature" section. The DEM that served as basis for this was the DEM of 2013-2014 provided on WalOnMap.

- **Flow accumulation - contributing area**
  The contributing area to flow accumulation was determined based on the DEM of 2013-2014 provided on WalOnMap. It was first filled using the "FillDepressionsPlanchonAndDarboux" function of the WhiteboxTools toolbox in QGIS. Then, the functions "D8Pointer" and "D8FlowAccumulation" of the same toolbox were used successively.

- **Tillage direction**
  Tillage direction was determined based on the interpretation of the orthophoto plans provided on WalOnMap between the years 2012 and 2021, with the assumption that the tillage direction corresponds to the sowing direction. First, the tillage direction was determined as its deviation compared to the North (corrected to range between 0 and 180°). Then, the difference between the aspect and this angle was taken in order to have for each pixel the angle between the aspect and the tillage direction.

- **Distance to field boundaries**
  The "distance to fields boundaries" variable was created using the "Euclidean distance" tool in QGIS. The field boundaries were determined based on the parcel maps between 2012 and 2022. Since some parcels were subdivided into smaller ones depending on the year, only the main parcels were taken into account.

- **R factor**
  The R factor is one of the parameters used in the USLE equation. It is used to represent the erosivity of the rainfall. To compute this parameter, the rainfall data sampled at a 5 minutes frequency in the catchment between 2012 and 2022 were used. Different methods and equations are encountered to compute the R-factor. The chosen method for this study is the Python $rfactor$ package (Gobeyn et al., 2021a), developed for Flanders (Belgium) (Gobeyn et al., 2021b). R is defined as the mean yearly rainfall erosivity factor ($MJ.mm.ha^{-1}.h^{-1}.year^{-1}$):

$$R = \frac{1}{n}\sum_{j=1}^{n}(\sum_{k=1}^{m_j} E_k(I_{30})_k)_j \tag{2.2}$$

  with j the index of the year considered, k the index of the rainfall event. $E_k(I_{30})_k$ or EI_{30} is the erosion index where E_k is the kinetic energy of the rainfall event ($J.m^{-2}$) and I_{30} is the maximum 30 minute intensity of an event ($mm.h^{-1}$).

  For each rainfall event k, E_k is computed as:

$$E = \sum_{r=1}^{o} e_r \Delta V_r \tag{2.3}$$

with r, the index of the data point in the time interval, o the number of data points, ΔV_r the amount of rain observed in a 10-minute time interval and e_r the unit rainfall energy ($J.m^{-2}.mm^{-1}$).

$$e_r = 11.12 \times i_r^{0.31} \tag{2.4}$$

where i_r is the rainfall intensity during the time interval of 10 minutes ($mm.h^{-1}$). Since the data available in the catchment are at a sampling resolution of 5 minutes, they have been resampled to a 10 minutes frequency prior to the R computation. Then, the rainfall erosivity index (EI_{30}) was computed and summed for each year in order to determine the R-value per year. The R factor is homogeneous in the catchment, and cannot be used as a variable to differentiate the parcels, but it will be used to compute the next variable, the C factor.

- **C factor**
  The C factor corresponds to the land cover and management factor of the USLE and RUSLE equation. According to Renard et al. (1997), it is computed as:

$$C = \frac{\sum_{i=1}^{n} SLR_i \times EI_i}{EI_{tot}} \tag{2.5}$$

where i refers to the time interval, EI is the rainfall erosivity index computed in the R factor and SLR corresponds to the Soil Loss Ratio:

$$SLR = PLU \times CC \times SC \times SR \times SM \tag{2.6}$$

with: PLU: Prio Land Use subfactor, CC: Canopy-Cover subfactor, SC: Surface-Cover subfactor, SR: Surface-Roughness subfactor, SM: Soil-Moisture subfactor. In this study, according to the methodology applied in Wallonia by Bielders et al. (2011), PLU and SM will be equal to 1. The PLU computation implies many different parameters that require long-term experimentation on field plots. The SM subfactor is also hard to compute. Its value is fixed at 1, considering that soil moisture is close to field capacity. The CC subfactor equals to:

$$CC = 1 - F_c \times e^{(-0.1.H)} \tag{2.7}$$

in which F_c is the fraction of soil covered by the canopy and H (ft) is the mean height at which raindrops fall after reaching the canopy. The SC subfactor is :

$$SC = e^{(-b \times S_p \times (\frac{0.24}{R_u})^{0.08})} \tag{2.8}$$

where b is an empirical coefficient (fixed to 0.035 (Bielders et al., 2011)), S_p is the percentage of soil covered by crop residues and R_u is the surface roughness (in), for $R_u \geqslant 0.24$ inches. The surface roughness is *"a function of the surface's random roughness, which is defined as the standard deviation of the surface elevations when changes due to land slope or nonrandom tillage marks (such as dead furrows, traffic marks, and disk marks) are removed from consideration"* (Allmaras et al. 1966, in (Renard et al., 1997)). The SR subfactor is computed as:

$$SR = e^{(-0.66 \times (R_u - 0.24))} \tag{2.9}$$

where R_u is still the surface roughness (in). The input values of the F_c and S_p parameters were derived from the FCR classification data according to table 2.3.

Table 2.3: F_c and S_p values derived from C factor (crop cover) of the FCR classification

Classes	**Percentage of area covered by either canopy or litter (%)**	**Value taken for F_c**	**Value taken for S_p**
C1	0-20	0.1	10
C2	21-60	0.4	40
C3	61-100	0.8	80

The value of H was derived for each date and crop type from the graphs produced in the study of Bielders et al. (2011). Since this study did not take into account the phacelia, the height of this crop was considered as linen. The plantation and harvest dates were assumed to be identical to the ones taken in this study. Another hypothesis is the fact that only the main crop was taken into account in this computation; since there was no sufficient information about the presence or type of an intercrop, the crop height was fixed to 0 before the sowing and after the harvest date. This is not supposed to have a large influence on the computation of the CC factor because the information of the canopy or litter cover (F_C) is still taken into account in the FCR classification. Moreover, the sensitivity analysis (figure 2.6) shows that for a low canopy cover, the height has a small influence on the CC value.

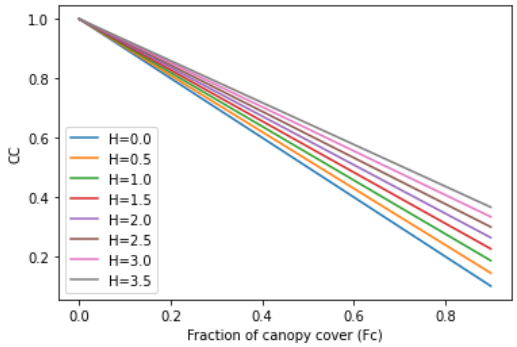

Figure 2.6: Sensitivity analysis of the influence of H on CC

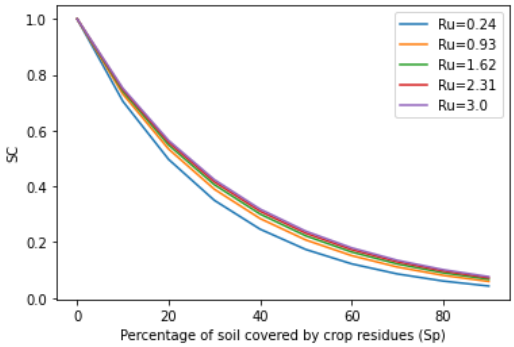

Figure 2.7: Sensitivity analysis of the influence of Ru (in inches) on SC

For the surface roughness, the roughness index of the FCR classification could not be used as input data since it does not correspond to the same type of roughness. Indeed, in the FCR classification, roughness is divided into classes from 0 to $>$ 15 cm and defined as the *"difference in the heights of the deepest part of microdepressions and the lowest point of their divide"* (Cerdan et al., 2001). This implies that in this case, the non random roughness (tillage and disks marks, ...) are taken into account and this is not in line with what is required for the R_u parameter in equations 2.8 and 2.9. Therefore, the roughness data were taken from the report of Bielders et al. (2011), in the same way as for H. The date ranges of the data is limited and the missing values were fixed to 0 (same for phacelia). Because equation 2.9 is only applicable for $R_u \geqslant 0.24$ and SR equals 1 otherwise, the SR parameter was equal to 1 most of the time.

For the SC parameter (equation 2.8), R_u was fixed to 0.24 inches, according to what was done in Bielders et al. (2011). Indeed, the sensitivity analysis (figure 2.7) shows that rugosity has a low influence on the value of SC.

For each date at which the FCR data were available, an SCR value was computed and multiplied by the EI computed in the R factor method (cumulated erosivity from the previous date). Then the products were summed for each parcel and divided by the total erosivity index (2013-2021).

The C factor computation covers the period 2013-2021.

The final output is a raster map (figure 2.8) where each parcel (or sub-parcel) gets a C value. For grass and woods, the map was completed with values taken from Cantreul et al. (2018), respectively 0.003 and 0.082.

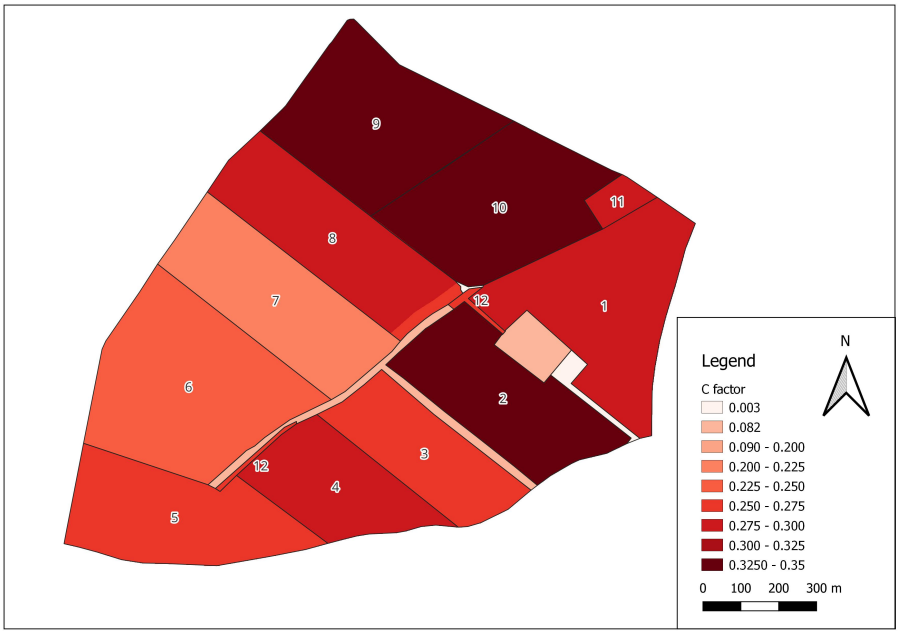

Figure 2.8: Map of the C factor and parcel numbers

- **IC (connectivity index)**
  The connectivity index (IC) can be calculated in a GIS environment. It represents the potential connectivity between the different parts of a watershed. It takes as input data an elevation map and weighting factors and is calculated as:

$$IC = log_{10}\frac{D_{up}}{D_{dn}} = log_{10}(\frac{\overline{W}\overline{S}\sqrt{A}}{\sum_i \frac{d_i}{W_i S_i}}) \tag{2.10}$$

  where D_{up} is the upslope component in which $\overline{W}$: average weighing factor of the upslope contributing area (dimensionless), $\overline{S}$: average slope gradient of the upslope contributing area (m/m), A: upslope contributing area (m^2) and D_{dn} is the downslope component with d_i: length of the ith cell along the downslope path (in m), W_i: weight of the ith cell (dimensionless) and S_i: slope gradient of the ith cell (m/m) (Borselli et al., 2008). The IC appears to depend on the pixel size, and was computed for this specific catchment by Cantreul et al. (2018). They determined that the most suitable pixel size is 1 m. To compute the IC factor, the methodology of Borselli et al. (2008) was applied using the Spatial Analyst extension of the ArcMap software, and according to what was done in both studies (Borselli et al., 2008; Cantreul et al., 2018), the C factor was used as weighting factor (W). The elevation map used was the WalOnMap DTM of 2013-2014.

- **LS factor**
  For the LS factor (slope length factor of the RUSLE equation), different options were investigated. It was first computed on QGIS with the LSfactor function of the 'SAGA > Terrain Analysis > Hydrology' tool. The input maps were a slope map (in radians) made with the same reference map as previously, the DTM of 2013-2014 provided on WalOnMap, and the catchment area. The method chosen was the algorithm of 'Desmet & Govers, 1996'. The other default parameters were kept unchanged. The second option was the LS map produced by the model WaTEM/SEDEM with the algorithm of Govers. The collinearity test (correlation matrix) between the variables will determine which of the two options will be kept in the statistical analysis.

- **Cultivation intensity**
  This last factor is not quantitative but a qualitative factor that was added to highlight

the differences in cultivation practices between the parcels. As shown in figure 2.2, some parcels experience more intense and shorter crop rotations than others, with an alternate between cereals and tuber crops such as sugar beet, potatoes, or chicory every 2 years. Those cultivation practices are likely to cause soil loss due to crop harvesting. In order to see if there was a difference in terms of erosion, the parcels with the shorter rotations of tuber crops were assigned a value of 2, the longer rotations had a value of 1 while the parcels that are always covered with maize had a value of 0.

2.4.2 Sampling method

An important objective of this study is to determine if there is a difference in terms of deposition in the rills and inter rills. To do so, a random sample of 500 points was produced in the catchment. The non-arable zones (forests and grass) were excluded from the analysis, as well as parcel n°10, where the gullies were filled by the farmer (see section 2.1).

2.4.3 Statistical analysis

Outliers detection

The first step of the analysis consisted in checking for outliers in the dependent variable in the datasets (the Difference of DEMs). To do so, the 25^{th} percentile ($Q1$) and the 75^{th} percentile ($Q3$) of the datasets were computed and enabled to determine the Interquartile Range (IQR). Then, each individual observation was analyzed and considered as an outlier if:

$$obs < Q1 - 1.5 \times IQR \quad or \quad obs > Q1 + 1.5 \times IQR \tag{2.11}$$

However, in order to avoid the loss of information associated with areas that potentially experience more erosion/deposition, this determination was followed by a visual interpretation of those outliers in the QGIS environment. Based on their respective values and in comparison with the values observed in the adjacent pixels, the points were removed from the dataset (considered as outliers) only if their value was considered as unlikely to represent erosion/deposition or if they were too different from the surrounding pixels.

Collinearity analysis

Then, a collinearity analysis was performed to test the correlation between the (quantitative) variables, by using a correlation matrix. The highly correlated variables were removed from the analysis.

Principal Component Analysis

After that, a Principal Components Analysis (PCA) was done on the dataset in R, using the FactoMineR library. This enabled us to see the relations between the variables and their potential contribution to explaining the phenomenon of erosion and deposition, as well as their possible interactions.

Multiple Linear Regression

Then, based on this, a Multiple Linear Regression (MLR) was carried out in R. It was divided into different steps, presented in figure 2.9. The principle of the MLR is to compute a linear regression based on the value of different independent variables in order to predict the value of the dependent variable. The MLR was performed on the same variables as the ones used in the PCA. The three DoD variables were successively considered as the dependent variable, while the rest were the independent ones. Different combinations of input variables were tested and

compared based on the value of the Akaike Information Criterion (AIC) and the adjusted R^2. The model with the highest adjusted R^2 and the lowest AIC was selected.

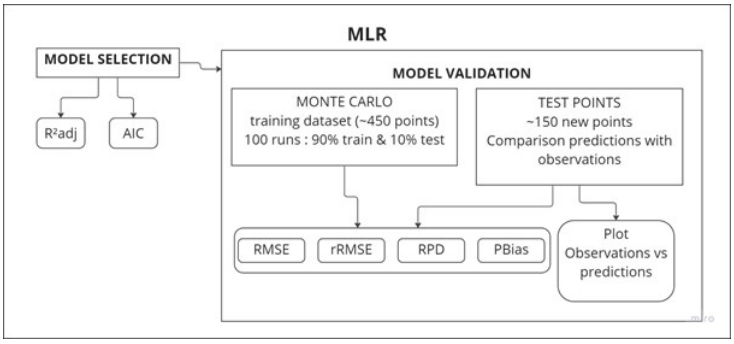

Figure 2.9: Flow chart of the Multiple Linear Regression

Model validation

Two types of model validation were performed. First, a Monte Carlo Cross-validation was carried out. It consists in running the model several times and having for each run a new sampling of a certain proportion of "train" and "test" data points. Then, it computes the mean value (over the x runs) of some parameters such as the Root Mean Squared Error ($RMSE$) of the model as well as its standard deviation. In this case, 100 repetitions were made, with 90% of "train" data and 10% of "test" data. In addition to this, other parameters such as the relative RMSE ($rRMSE$), the Ratio of Performance to deviation (RPD) and the percent bias ($PBias$) were extracted and computed as follows:

$$RMSE = \sqrt{\frac{\sum(x_{obs} - x_{pred})^2}{n_{obs}}} \tag{2.12}$$

where x_{obs} and x_{pred} are the observed and predicted values of erosion/deposition, respectively and n_{obs} is the number of observations.

$$rRMSE = \frac{RMSE}{\overline{x_{obs}}} \tag{2.13}$$

where $\overline{x_{obs}}$ is the mean value of the observations.

$$RPD = \frac{\sigma_{obs}}{RMSE} \tag{2.14}$$

with σ_{obs}, the standard deviation of the values observed.

$$PBias = \frac{\sum(x_{pred} - x_{obs})}{\sum x_{obs}} \times 100 \tag{2.15}$$

The second validation approach consisted of sampling about 120 new random points in the catchment and using the model to predict their deposition/erosion based on the value of the independent variables. Then, the predictions were compared to the observations and the quality of the predictions were assessed trough the values of the $RMSE$, $rRMSE$, RPD, and $PBias$. The analysis was performed separately for the 3 Differences of DEM data sources (WalOnMap (DTM and DSM) and drones).

2.5 WaTEM/SEDEM Modeling

2.5.1 General settings description

For the WaTEM/SEDEM modelings, different input parameters are needed (description adapted from Notebaert et al. (2006)):

- **Elevation map**
- **Parcel map**: each parcel is numerated from 1 to n, and some values are assigned for each land use type: -2: roads and build-up area, -1: rivers, 10000: forests, 20000: pasture, 0: outside the studied area.
- **River routing map** (optional)
- **Crop factor** - C factor (RUSLE): can be either a value (identical for the entire catchment) or a map. The default value is 0.37 for croplands, 0.001 for forests and 0.01 for pasture.
- **Ponds**: location of ponds or retention pools in the area.
- **Soil erodibility factor** - K factor (RUSLE): can be either a value (identical for the entire catchment) or a map. The default value is 35 (expressed in $kg.m^{-2}.h.MJ^{-1}.mm^{-1}$).
- **Ptef: Parcel**: can be either a value (identical for the entire catchment) or a map: *"represents how much a given pixel contributes to water transport, compared with a referential base (plain arable land)"*. The default value is fixed to 0 for cropland and 75 for both pasture and forest.
- **Parcel connectivity**: can vary between 0 and 100 and *"represents to what extent water transport is stopped at the parcel border"*. It means that for a value of 90, 10% of the water can reach the adjacent parcel. The default values are set to 10 for a connection to croplands and 75 for pasture and forest.
- **Rainfall erosivity** - R-factor (RUSLE): value expressed in $MJ.mm.m^{-2}h^{-1}$. The default value is 0.087.
- **Transport capacity coefficient** (k_{TC}): maximum sediment mass that can be transported in a pixel. A low, high and limit value can be adapted. Default values are 75, 250 and 0.1, respectively.
- **Slope length factor** - LS (RUSLE): different options for the algorithm to use.
- **Tillage transport coefficient** (k_{till}): 600 kg/m^2
- **Bulk density**: a constant value on the whole catchment, with as default value 1350 kg/m^3

For the different modelings, the spatial resolution is 20m, which is the default resolution in WaTEM/SEDEM. The elevation map was the DTM WalOnMap 2013-2014, resampled to 20m resolution. Since the model was built for Flanders, the default values of the different input parameters are supposed to be close to what we could expect for Wallonia. However, the model is aging and the more recent computations of those parameters show differences with the default values included in WaTEM/SEDEM. Therefore, the following input parameters were adapted:

- **K factor**(soil erodibility): the latest computation of this factor was performed in 2022 by Maugnard et al. (2022). Based on the maps produced in the report, the value of 0.06 $t.h.MJ^{-1}mm^{-1}$ was chosen. This value had to be converted in $kg.h.m^{-2}.MJ^{-1}mm^{-1}$ to match the requirements of WaTEM SEDEM. This results in a value of 60 $kg.h.m^{-2}.MJ^{-1}mm^{-1}$.
- **R factor**(rainfall erosivity): still according to the report of Maugnard et al. (2022), a value of approximately 750 $MJ.mm.m^{-2}.h^{-1}$ was selected, resulting in 0.075 $MJ.mm.m^{-2}.h-1$

for WaTEM SEDEM.

The output maps representing water erosion, tillage erosion, and total erosion can be expressed in ton/ha or in mm. In this study, we use the mm in order to simplify the comparison with the DoDs that are expressed in m. The model also provides the total sediment production, the total sediment deposition, and the total sediment export (in t). The different outputs will be compared.

2.5.2 Influence of the connectivity

First, the influence of the parcel connectivity was tested. The connectivity to cropland was set to 0, 30, 50, 70, and 100. The parcel map (figure 2.10) was created in the same way as for the tillage direction, taking into account the parcel division which is the most often observed through the years.

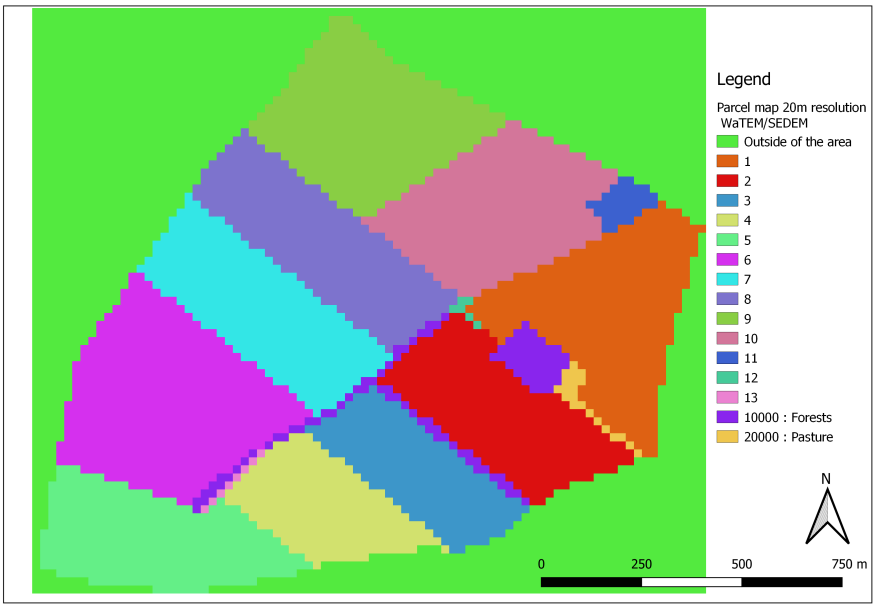

Figure 2.10: Parcel map 20m resolution used as input in WaTEM/SEDEM

The rest of the input parameters were kept to the default values.

2.5.3 Influence of parcel division

Then, in order to test the influence of the parcel division in the modeling, several runs were made using different values of connectivity (0 and 100) with the catchment considered as one unique parcel (figure 2.11).

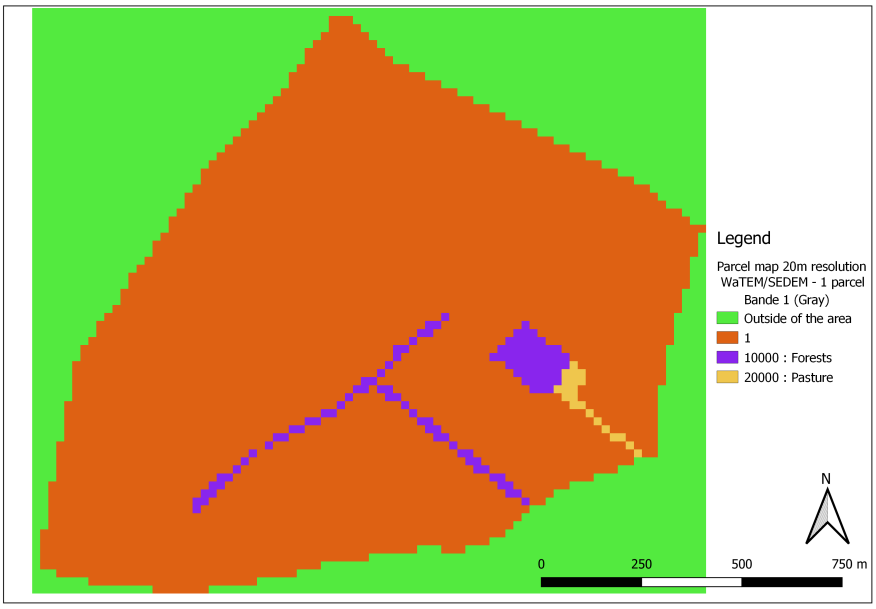

Figure 2.11: Parcel map 20m resolution used as input in WaTEM/SEDEM (homogeneous catchment)

2.5.4 Adaptation of the C factor

In this section, the influence of the C factor was tested, by replacing the default value of 0.37 by the map produced for the catchment (section 2.4.1), with an individual value for each parcel. The connectivity was set to 70, as the most common connectivity value considered nowadays in Belgium is 30%. As a reminder, in our case, a connectivity value of 70% corresponds to 30% of water transferred to the next parcel. This run is supposed to be the closest to reality.

2.5.5 Influence of filling the DTM

For this last trial, the exact same input parameters were used as in the previous section, except for the DTM that was first filled using the functions presented in section 2.4.1.

2.6 Evolution of the streams in the catchment

One advantage of this experimental catchment is the fact that it is now followed for a relatively long period (around 10 years). The frequent fields surveys and the monitoring of the different devices present in the catchment enabled to follow the catchment closely. This was done by Gilles Swerts who witnessed some changes in the flow paths around the years/ seasons, depending among others on the agricultural practices. Since different DEM sources are also available, a test was made to see if those changes in flow paths were also visible with the DEMs at 1m resolution. So, in addition to the flow accumulation map produced for the WalOnMap DTM of 2013-2014, several flow accumulation maps were produced based on the WalOnMAp DTM of 2021-2022 and UAV DTM of 2022, using the same QGIS functions (see section 2.4.1). For the WalOnMap DTM of 2021-2022 that was in Lambert 2008 (EPSG:3812), the flow accumulation was first produced and then reprojected in Lambert 72 (EPSG:31370), because doing the opposite (reproject the DTM first) produced unexpected results.

2.7 Comparison of the model approach and the difference of DEMs

We will compare the modeling approach using WaTEM/SEDEM with the DoD by different means. First, a visual interpretation will be performed by comparing the output map of WS considered as the most realistic (parcel division, connectivity set to 70%, C map and DTM not filled) with the DoDs. Diverging as well as converging zones will be visually compared. Then, we will quantify the proportion of deposition occurring in the inter-rills and in the rills in the DoDs. To do so, different zones were defined in the catchment as shown in figure 2.12. The rills zone was created by using a 10m buffer around the accumulation flows. The inter-rills zone corresponds to the rest of the catchment. Note that the vegetated zone was removed from the analysis in both zones. For each zone (rills and inter-rills), the sum of the deposition was computed and then divided by the area of the zone. This corresponds to the mean value of deposition. Then, the mean deposition in the rills was divided by the mean deposition in the rest of the catchment.

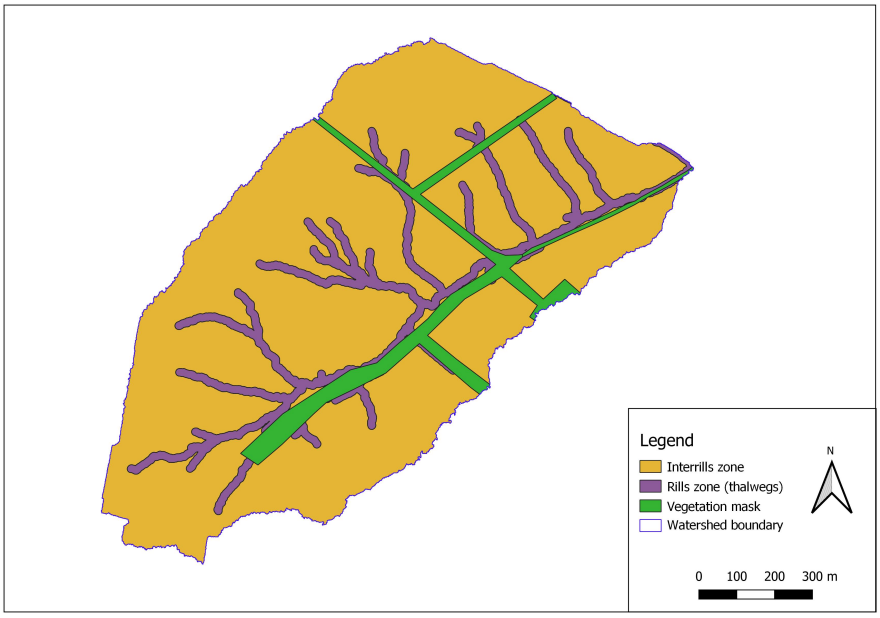

Figure 2.12: The zones defined to characterize the distribution of deposition in the catchment

Chapter 3

Results

3.1 DEM analysis

3.1.1 Influence of the vegetation

A visual analysis of 5 transect lines chosen arbitrarily in the catchment (figure A.1 in the appendix) to compare the elevation differences between the DSM and DTM shows that for the WalOnMap data, the influence of vegetation is particularly high in the strips of vegetation. For example, in line 4, an important peak can be observed in the DSM (figures 3.1 and 3.2). Therefore, to avoid misinterpretation of the elevation changes values, the vegetation strips will be excluded from the statistical analysis.

Since the only UAV-sourced data for which the DTM and the DSM are present is the year 2022, a comparison was also made for this year (figure 3.2). It shows higher differences between the DSM and the DTM, even outside the vegetation strips. This can be explained by the fact that the flight occurred in April 2022, which implies that vegetation was also present in the fields, which influences the elevation value in the DSM. In order to avoid this effect, it would be logical to choose the DTM instead of the DSM for the UAV data. However, a comparison between the WalOnMap and UAV data was carried out with the same transects (figure 3.4), and for 2022, the DTM appears to be the most different from the other data sources. For 2013, the UAV DSM tends to be similar to both the DSM and the DTM of WalOnMap (figure 3.3).

3.1.2 Uncertainty analysis

The location of the points taken for the comparison on the road and path is shown in figure 3.5. The elevation of the pixel in the different rasters is shown in table 3.1. The differences of elevation compared to the WalOnMap DTM of 2013-2014 is shown in table 3.2. The average of the absolute difference and the standard deviation were computed for each dataset, after having removed the eventual NAs. Except for the UAV DTM of 2022, the differences remain globally lower than the precision in Z (see table 2.2), which is encouraging regarding the reliability of the data sources. The higher differences in elevation with the UAV DTM of 2022 are in line with the observations of the transect approach (section 3.1.1). This is another argument to use the DSM of 2022 instead of the DTM for the UAV, even if the acquisition dates are not similar as is normally required.

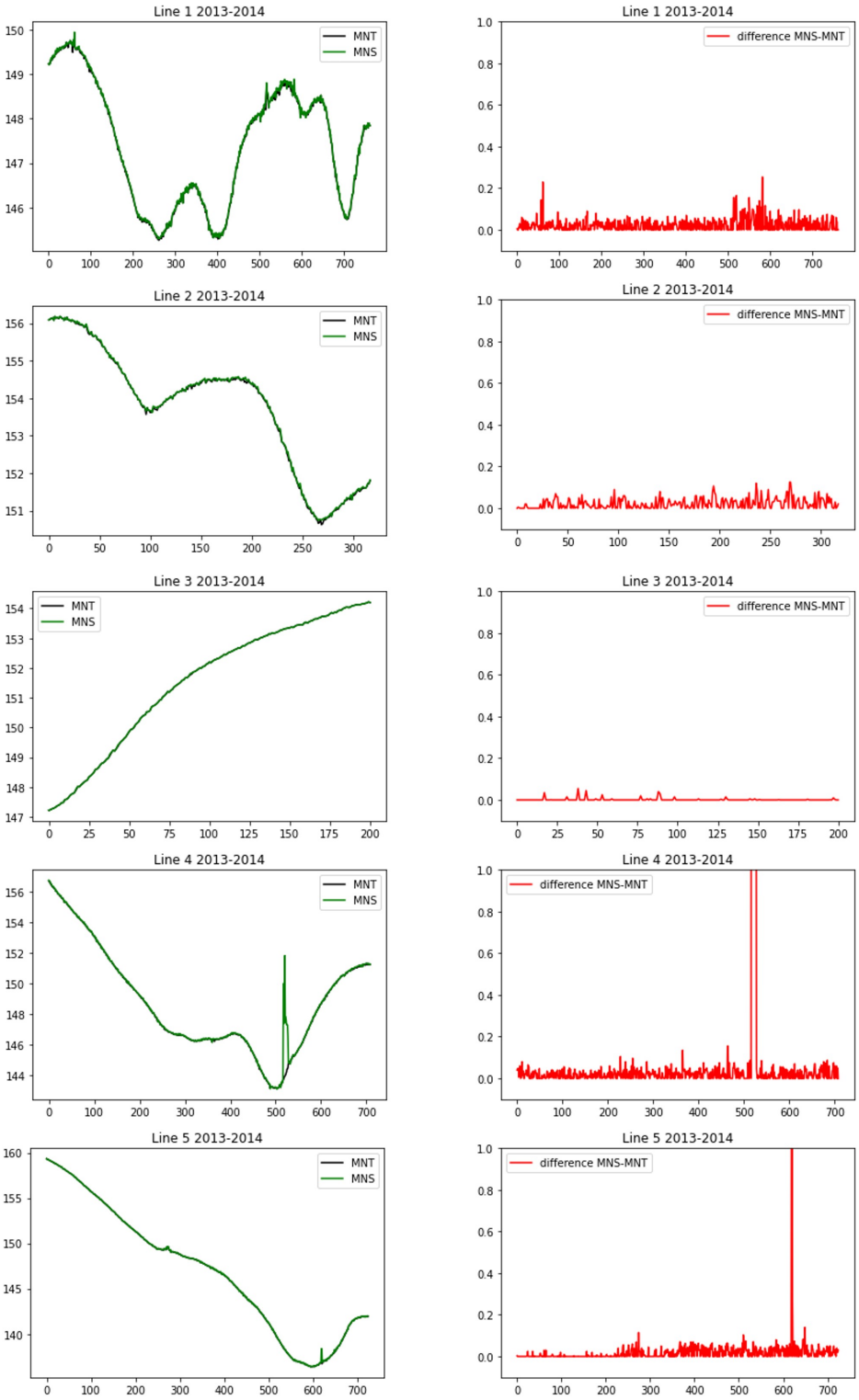

Figure 3.1: Differences between the DTM (mnt) and DSM (mns) of the transect lines for WalOnMap data of 2013-2014

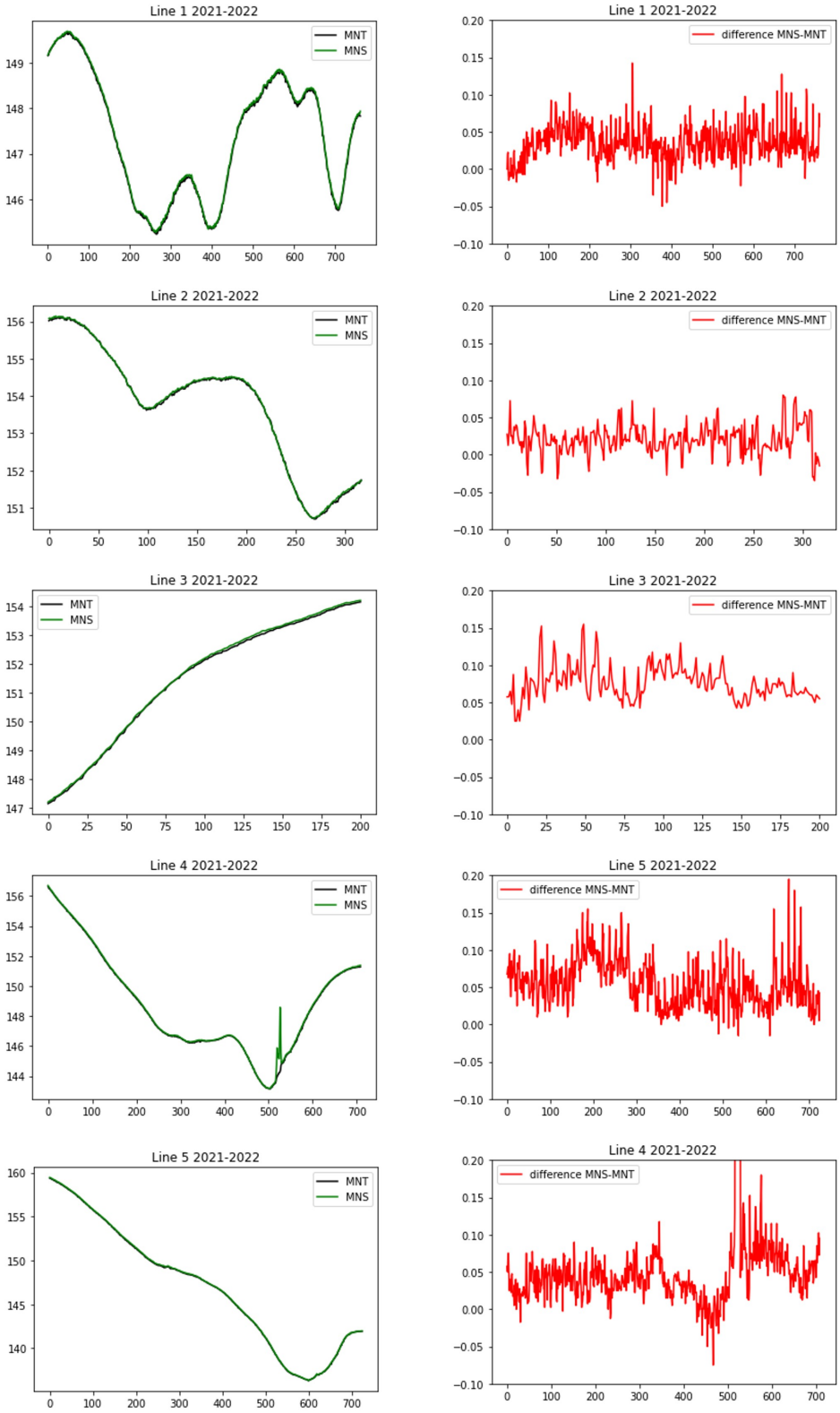

Figure 3.2: Differences between the DTM (mnt) and DSM (mns) of the transect lines for WalOnMap data of 2021-2022

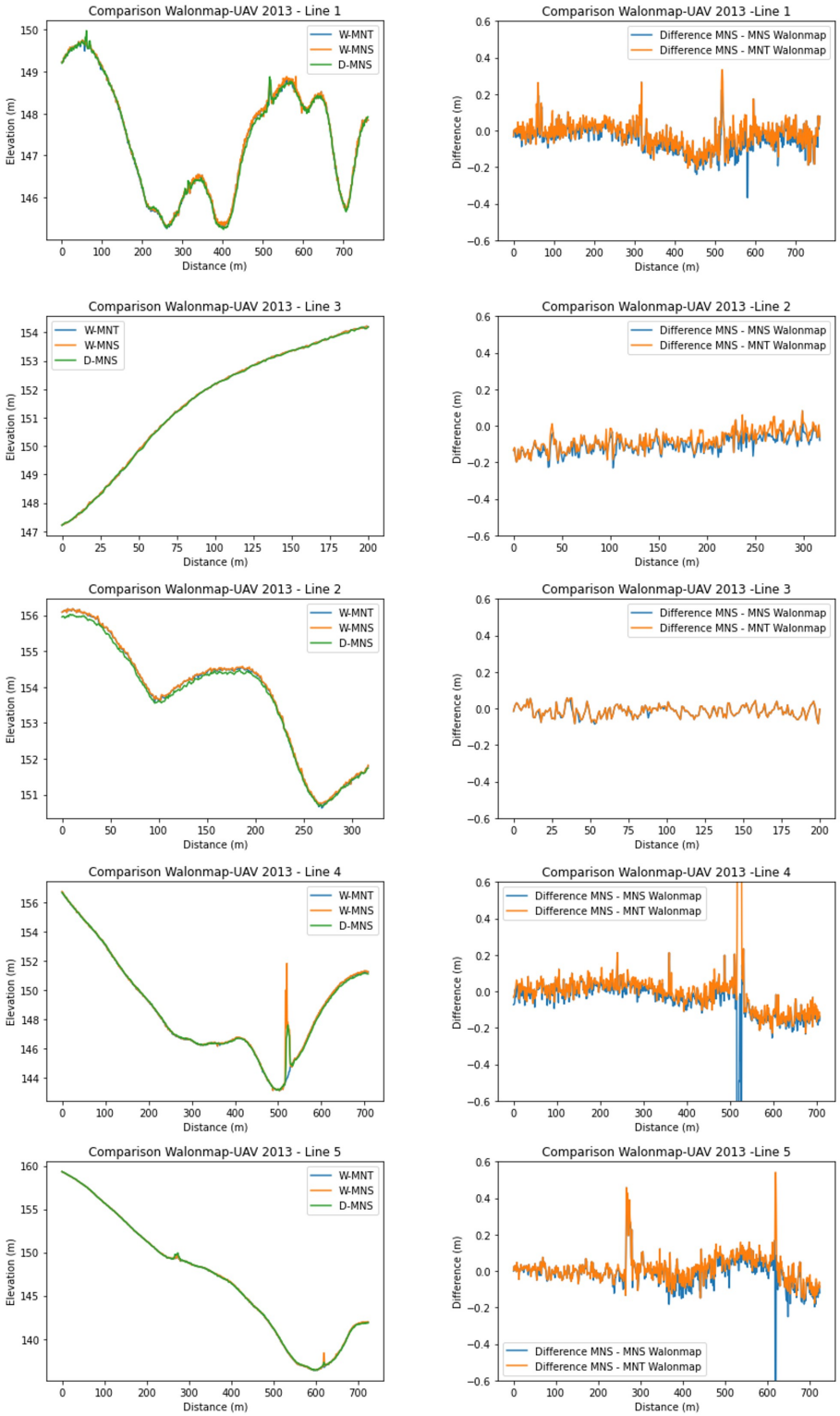

Figure 3.3: Differences between the DTM (mnt) and DSM (mns) of the transect lines for WalOnMap data of 2013-2014 and the drone DSM of 2013

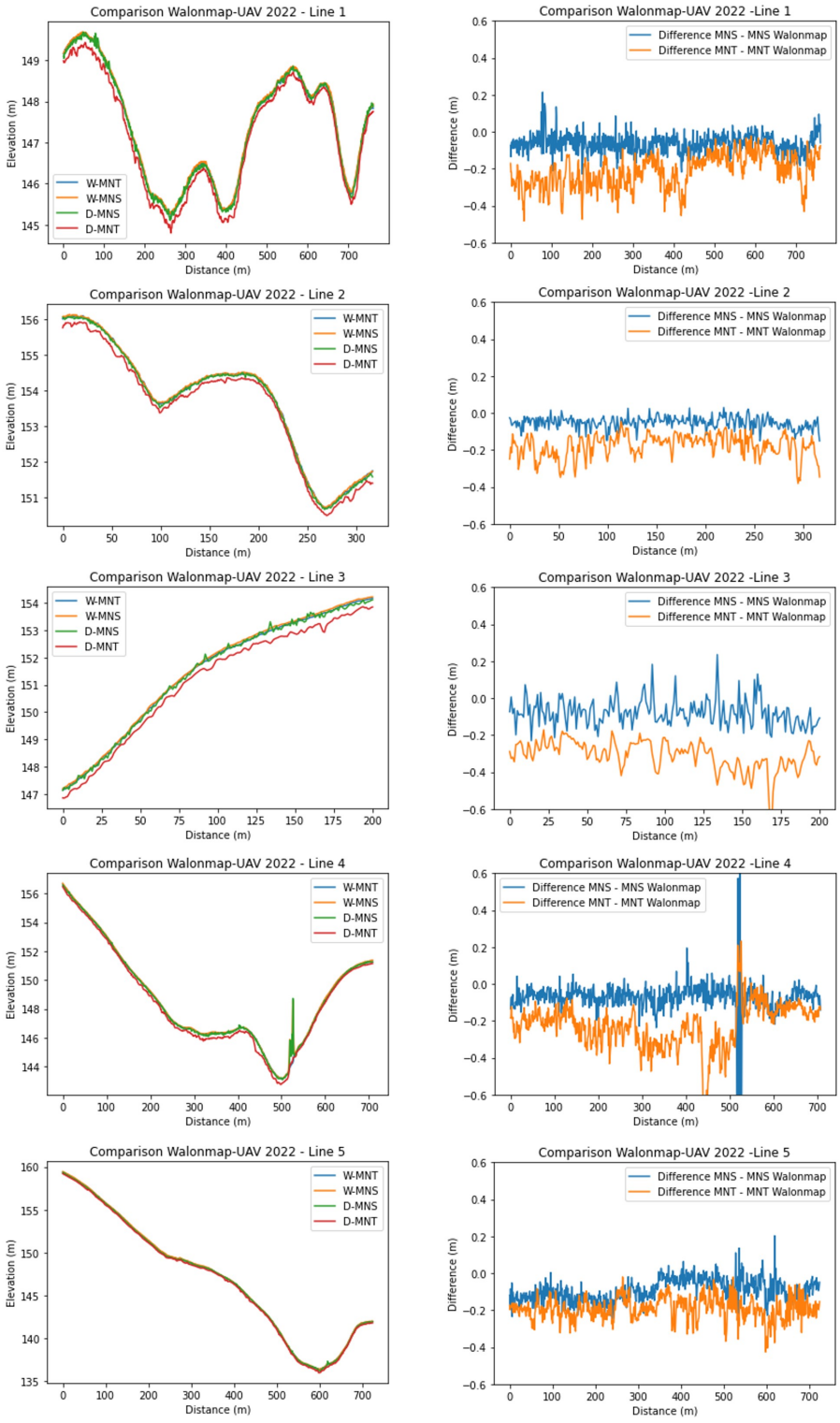

Figure 3.4: Differences between the DTM (mnt) and DSM (mns) of the transect lines for WalOnMap of 2021-2022 and drone data of 2022

Figure 3.5: Location of the "control points"

Table 3.1: Elevation (in m) of the "Control points" in the different DEM data sources

	UAV			WalOnMap			
id	DSM 2013	DSM 2022	DTM 2022	DSM 2013	DTM 2013	DSM 2022	DTM 2022
1	144.01	143.99	143.83	143.98	143.98	144.06	144.03
2	135.42	135.48	135.23	135.43	135.43	135.47	135.42
3	NA	129.98	129.79	130.06	130.01	130.04	129.98
4	155.19	155.16	155.02	155.19	155.19	155.26	155.19
5	159.18	159.21	159.00	159.21	159.21	159.29	159.22
6	158.18	NA	NA	158.18	158.18	158.20	158.17
7	158.13	NA	NA	158.08	158.07	158.14	158.08
8	158.90	NA	NA	159.00	159.00	159.04	159.00
9	157.44	157.50	157.36	157.57	157.57	157.67	157.57
10	158.72	158.91	158.74	159.01	159.01	158.99	158.96
12	158.25	158.24	158.11	158.46	158.46	158.29	158.24
13	154.47	154.45	154.06	154.51	154.50	154.58	154.50
14	155.40	155.32	155.11	155.41	155.40	155.46	155.39

Table 3.2: Elevation differences (in m) of the "Control points" in the different DEM data sources, compared to DTM WalOnMap 2013-2014

	UAV			WalOnMap			
id	DSM 2013	DSM 2022	DTM 2022	DSM 2013	DTM 2013	DSM 2022	DTM 2022
1	0.029	0.008	-0.155	0.000	0.000	0.080	0.053
2	-0.008	0.049	-0.198	0.000	0.000	0.040	-0.007
3	NA	-0.034	-0.223	0.050	0.000	0.033	-0.032
4	0.003	-0.032	-0.169	0.000	0.000	0.072	0.000
5	-0.025	0.003	-0.206	0.000	0.000	0.080	0.007
6	-0.005	NA	NA	0.000	0.000	0.023	-0.012
7	0.054	NA	NA	0.005	0.000	0.063	0.005
8	-0.099	NA	NA	0.000	0.000	0.038	-0.003
9	-0.130	-0.075	-0.206	0.000	0.000	0.100	0.003
10	-0.294	-0.104	-0.268	0.000	0.000	-0.025	-0.048
12	-0.212	-0.221	-0.346	0.000	0.000	-0.170	-0.215
13	-0.030	-0.047	-0.442	0.010	0.000	0.080	0.003
14	-0.001	-0.084	-0.298	0.005	0.000	0.053	-0.015
mean	0.068	0.051	0.193	0.005	0	0.066	0.031
sd	0.105	0.075	0.089	0.014	0	0.070	0.063

3.1.3 Difference of DEM

Based on the DEM analysis performed in section 3.1.1 and 3.1.2, three Differences of DEMs (DoDs) maps were produced (figure 3.6): the differences between the UAVs DSM of 2022 and 2013 (a), the differences between the WalOnMap DTMs of 2021-2022 and 2013-2014 (b), and the differences between the WalOnMap DSMs of 2021-2022 and 2013-2014 (c). The different DoDs are also presented separately in the annex (figure A.2, A.3, A.4). As a reminder, positive values (blue) are assigned to deposition while negative values (red) correspond to erosion (section 2.3.3). Our first observation is that, on the perspective of the whole catchment, the two data sources (drones versus WalOnMap) do not show the same tendencies in terms of the spatial distribution of erosion and deposition. The range of erosion and deposition seems to be higher for the drone DoD than for the WalOnMap DoD.

On the drone DoD, we observe deposition in the upper parts of the catchment, as well as in the lower parts of some parcels.

The DTM DoD shows erosion in most of the catchment and deposition in parcels 8, 9, 10, and 11. In both cases, we observe that deposition is not only located in the rills as it is the case in the WS modeling. The DSM DoD shows the same tendencies as the DTM DoD, but seems to be influenced by eventual different flight dates since we observe lines that do not seem to represent reality. For each DoD, some statistical parameters (mean, standard deviation, minimum and maximum values) were computed with the zonal statistics tool in QGIS. This was done for the whole catchment area and for the catchment without the vegetation strips (mainly areas covered with trees), by using a mask. The results are shown in table 3.3.

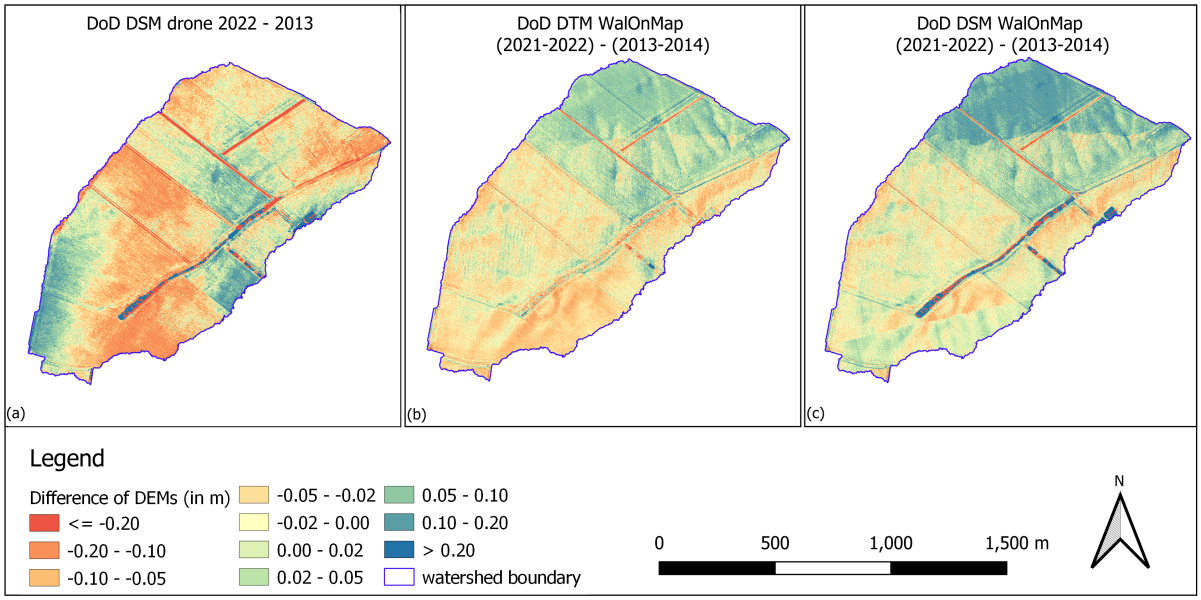

Figure 3.6: Differences of DEMs (DoD)

When comparing the statistical parameters for the whole catchment and for the catchment without vegetation, we see that the main difference is observed in the minimum and maximum values, especially for the DSMs. This also results in a reduction of the standard deviation. This distinction was made in order to capture what were the main tendencies observed in the fields in terms of erosion and deposition. The mean and median values remain small (not more than a few centimeters). This also enables us to see that even when removing the most sensitive zones (trees), some extreme values remain in the DoD, as we can see in the minimum and maximum values that are not likely to represent real soil erosion or deposition. Therefore, it will be necessary to check for eventual outlier values prior to the statistical analysis.

Table 3.3: Zonal statistics of the different DoDs (values expressed in m)

	DoD source	mean	sd	min	max
Total catchment	DTM Walonmap	-0.001	0.060	-1.443	0.651
	DSM Walonmap	0.033	0.452	-15.891	17.851
	drone	-0.005	0.526	-11.197	17.350
Catchment without vegetation strips	DTM Walonmap	0.000	0.058	-1.443	0.651
	DSM Walonmap	0.020	0.174	-15.971	8.666
	drone	-0.029	0.096	-1.159	6.155

3.2 Statistical analysis

3.2.1 Variables

The different variables maps are presented in the appendix (figure A.10). Note that the flow accumulation variable was presented as its log_{10} in order to improve the visual interpretation only.

3.2.2 Outliers detection

The histograms of the DoD values of the points are presented in figure 3.7. A boxplot of the DoD values is presented in figure A.5 in the appendix.

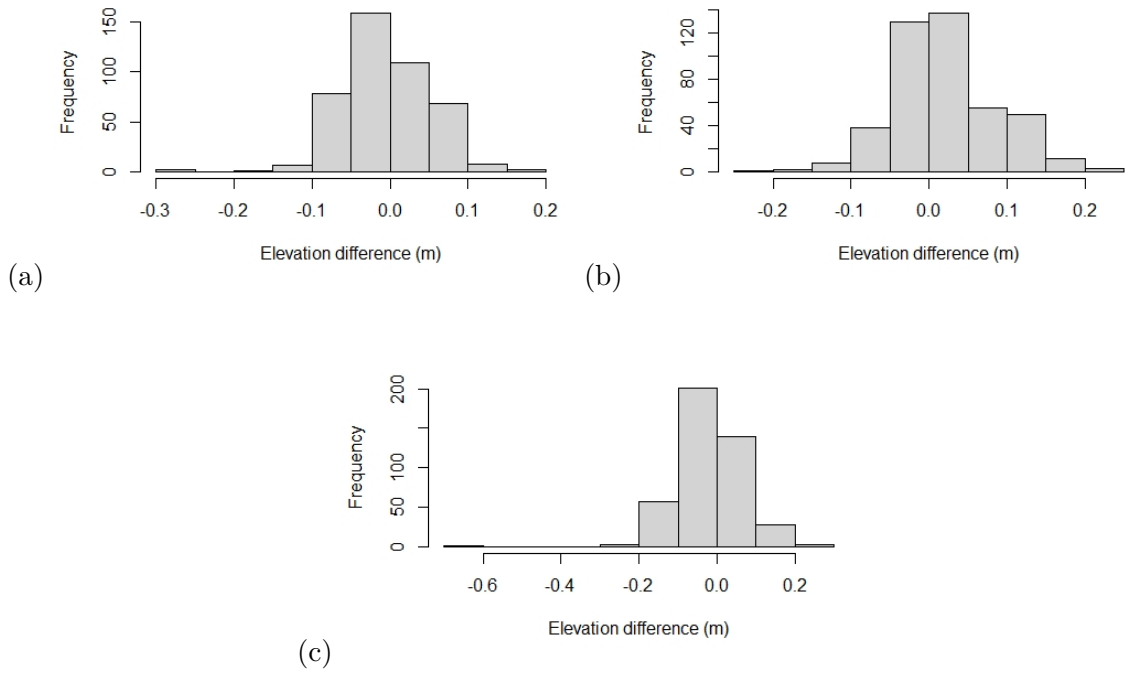

Figure 3.7: Histograms of the DoD values (in m) of the sampling points: (a) DTM WalOnMap , (b) DSM WalOnMap and (c) drone DSM

We can observe that the distribution is normal and concentrated between -10 and 10 cm, but some points present higher values. Therefore, an outliers analysis was conducted. The comparison of the DoD to the IQR enabled to spot 15 points as outliers (figure 3.8). However, an inspection of those data showed that an important part of the points identified as outliers were located near the field boundaries. The value of their erosion or deposition was checked and compared to the surrounding pixel values of the DoD maps. If the values were not too different, the point was kept in the analysis and removed from the outliers. If the value seemed to be highly influenced by the field boundaries and by the depressions or bumps caused by the mechanical engines, or by the ancient presence of a grass strip, the point was considered as an outlier. This resulted in only 5 points considered as outliers.

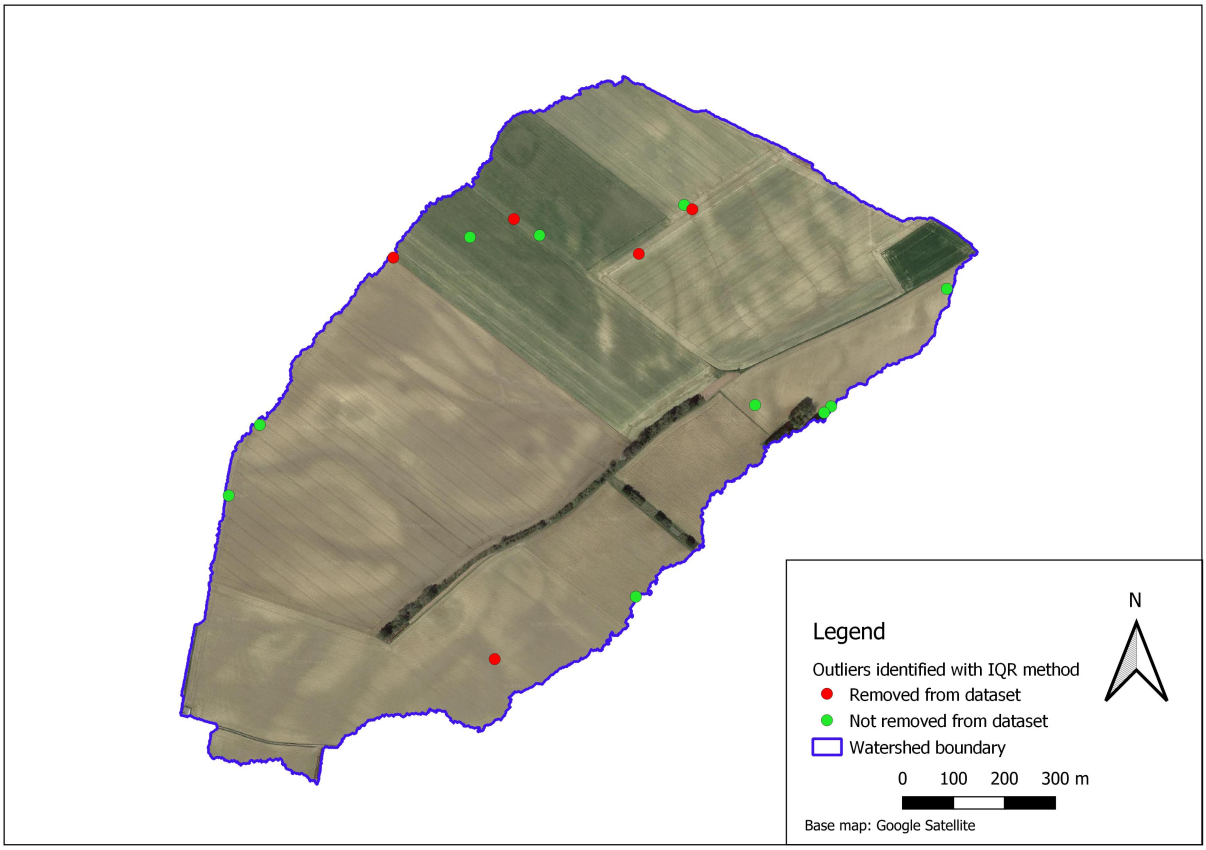

Figure 3.8: Outliers detection

3.2.3 Colinearity between the variables

The correlation matrix (table 3.4) revealed that the slope and the LS were highly correlated. Since two options were available for the LS, only the one with the lowest correlation with the slope was kept for the statistical analysis (LS computed with WaTEM/SEDEM). The two WalOnMap DoDs are also highly correlated but this was expected and is not a problem since the multiple linear regression will be made separately for the different dependent variables.

Table 3.4: Correlation matrix of the variables

	C factor	curvature	distance to field boundaries	DoD drone	flow accumulation	IC	LS (WaTEM/ SEDEM Govers)	LS (SAGA)	DoD DSM	DoD DTM	slope	tillage direction
C factor	1.000											
curvature	-0.017	1.000										
distance to field boundaries	0.018	-0.049	1.000									
DoD drone	0.032	-0.046	0.027	1.000								
flow accumulation	-0.079	-0.046	0.057	0.015	1.000							
IC	0.066	-0.121	0.037	0.009	0.047	1.000						
LS (WaTEM/ SEDEM Govers)	0.082	-0.020	0.000	0.005	-0.020	0.486	1.000					
LS (SAGA)	0.026	0.041	0.056	-0.041	-0.043	0.507	0.526	1.000				
DoD DSM	0.478	-0.366	0.162	0.104	0.010	0.022	-0.033	-0.238	1.000			
DoD DTM	0.404	-0.498	0.218	0.239	0.030	0.087	-0.048	-0.169	0.872	1.000		
slope	0.007	0.038	0.044	-0.034	-0.068	0.491	0.511	0.972	-0.263	-0.185	1.000	
tillage direction	0.098	0.069	-0.222	0.081	-0.050	0.129	0.225	0.255	-0.300	-0.291	0.278	1.000

3.2.4 Principal components analysis

The principal component analysis (PCA) used 11 variables, including one qualitative variable (the cultivation intensity) and 10 quantitative variables listed here with the corresponding abbreviations used in the figures.

- DoD DTM WalOnMap: `mnt`
- DoD DSM WalonMap: `mns`
- DoD DSM drone: `drone`
- Slope: `slope`
- LS factor: `LS-gov`
- Tillage direction: `till-dir`
- Flow accumulation: `flowacc`
- Curvature: `curvature`
- Index of connectivity: `IC`
- C factor: `C`
- Cultivation intensity: `cult-int`

In the first step of the analysis, the plots of the individuals on the different axes were analyzed to spot potential outliers (figure 3.9).

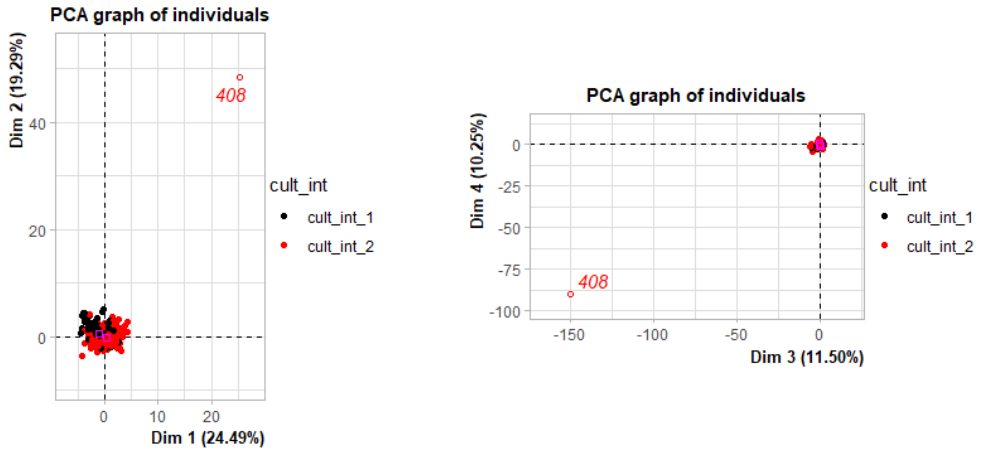

Figure 3.9: Plot of the individuals on the dimensions 1 and 2 (left) and 3 and 4 (right)

The point 408 was identified as such and considered as an outlier in the rest of the analysis. Then, the correlation circles (figure 3.10) were produced and the correlations between the variables and the principal components (the axes) were computed. The correlation circles of the other main axes are presented figure A.6 in the appendix. The plot of the "eigenvalues" (figure 3.11) of each principal component revealed that most of the information is in the first and the second components, but the 4 first components (corresponding to the dimensions or axes in the circles of correlation) can be retained in the analysis (eig > 1).

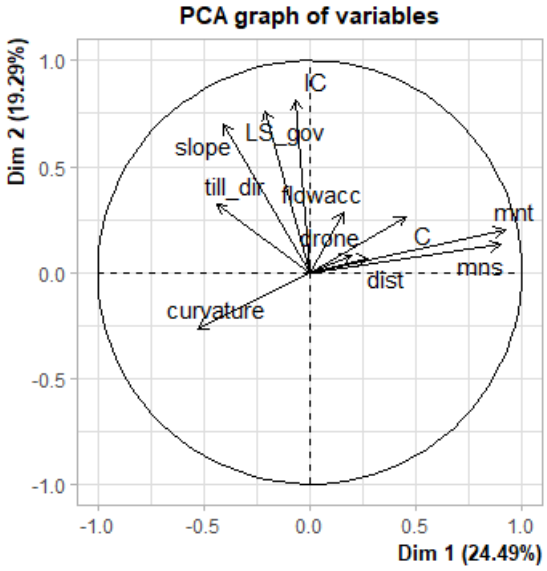

Figure 3.10: Circle of correlation on the 2 first axes

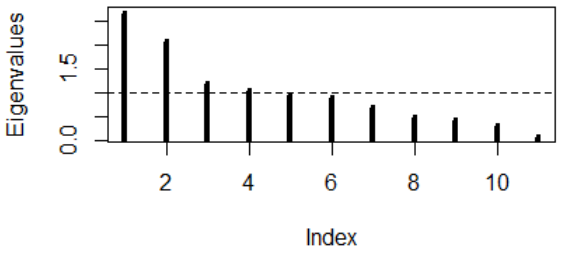

Figure 3.11: Graph of the 'eigenvalues' of the principal axes of the PCA

The values of the correlation of the variables with the principal components that have a high significance level (p-value ≤ 0.05) are shown in the annex (figure A.7). The observation of the correlation circles combined with the value of the correlation between the variables and the principal dimensions show that on the first dimension `mnt` and `mns` are highly correlated to each other, and are also correlated to the `C factor` and negatively correlated to the `curvature`. On the second dimension, we observe a correlation between the `IC`, the `slope` and `LS`. This correlation might imply an interaction between the variables, that will be tested in the MLR. The plots of the individuals (after removing point 408) with a distinction between the modalities of the "cultivation intensity" factor (figure 3.12) did not show a clear contrast in the distribution of the points along the axes.

Table 3.5: Model selection - multiple linear regression

		Variables										Parameters	
	model n°	C	curvature	dist	flowacc	IC	LS_gov	slope	till_dir	cult_int	slope*IC	slope*LS_gov	R^2-adj	AIC
DTM	**M1**	x***	x***	x***	x*	x***	x	x***	x***				0.527	-1605.6
	M2	x***	x***	x**	x .	x**	x	x***	x	x***			0.620	-1698.1
	M3	x***	x***	x***	x*	x***		x***	x***				0.528	-1607.6
	M4	x***	x***	x***	x*	x*	x	x***	x***		x		0.526	-1603.8
	M5	x***	x***	x***	x*	x**	x	x**	x***			x	0.526	-1604.0
	M6	x***	x***	x**	x .	x	x	x	x	x***	x	x	0.618	-1694.4
DSM	**M1**	x***	x***	x*	x*	x*	x .	x***	x***				0.505	-1425.6
	M2	x***	x***	x	x	x .	x *	x***	x	x***			0.601	-1516.3
	M3	x***	x***	x*	x*	x**		x***	x***				0.502	-1424.1
	M4	x***	x***	x*	x*	x.	x.	x***	x***		x		0.504	-1423.8
	M5	x***	x***	x*	x*	x*	x.	x***	x***			x	0.505	-1424.8
	M6	x***	x***	x	x	x	x	x**	x	x***	x	x	0.600	-1514.1
drone	**M1**	x	x	x	x	x	x	x	x*				0.002	-989.3
	M2	x	x	x	x	x	x	x .	x	x			0.003	-988.9
	M3								x.				0.004	-997.2
	M4	x	x	x	x	x	x	x	x *		x		0.000	-987.4
	M5	x	x	x	x	x	x	x	x*			x	0.000	-987.3
	M6	x	x	x	x	x	x	x	x	x	x	x	-0.001	-984.9

legend: x:variable included in the model, level of significance of the variable: ∗ ∗ ∗ (p-val<0.001), ∗∗ (p-val <0.01), ∗ (p-val<0.05), . (p-val<0.1).

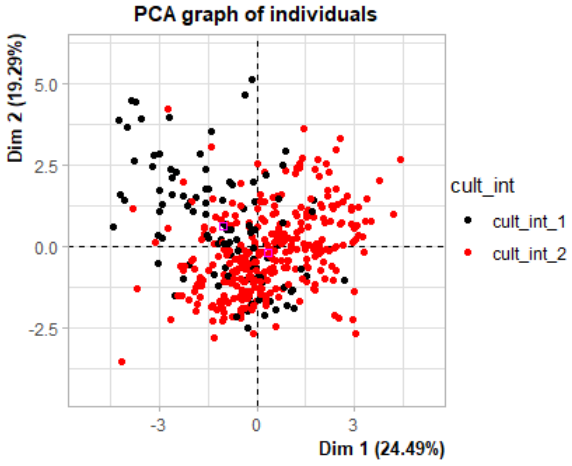

Figure 3.12: Plot of the individuals with distinction based on the variable 'cultivation intensity'

3.2.5 Multiple linear regression

The different variables combinations and the performance parameters associated are presented in table 3.5.

The different models can be explained as follows:

- **M1** All the quantitative variables
- **M2** All the quantitative variables and the qualitative variable (cultivation intensity)
- **M3** Only the quantitative variables that were at least significant (p-value ≤ 0.05) in the first run
- **M4** All the quantitative variables and the interaction term between slope and the IC factor
- **M5** All the quantitative variables and the interaction term between slope and LS factor
- **M6** All the variables and the 2 interaction terms

For the Walonmap datasets (DTM and DSM), the second model (M2) was selected. For the drone dataset, none of the models performed really well. Indeed, the model with the highest

adjusted R^2 (remaining low) and the lowest AIC had only one independent variable. Therefore, the same model as for Walonmap was chosen in order to enable comparison.

3.2.6 Model validation

The results of the Monte Carlo validation are presented in table 3.6 and figure 3.13. Note that since the values are computed for each of the 100 runs, only the mean values of the parameters are presented in this section. The boxplots presenting the variation observed over the different runs are presented in figures A.8 in the appendix.

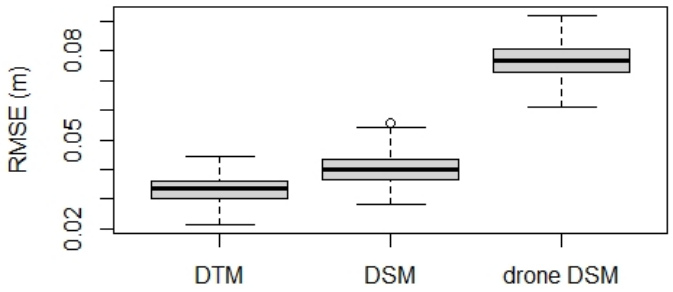

Figure 3.13: Boxplots of the RMSE (in m) of the Monte Carlo validation over 100 runs for the three datasets

Table 3.6: Mean values of the parameters of the Monte Carlo validation

source	RMSE (m)	rRMSE (-)	RPD (-)	Pbias (%)
DTM	0.033	-12.272	1.625	22.5
DSM	0.040	2.202	1.584	-5.4
drone	0.077	-4.639	1.000	5.7

The results of the 'testing' points validation are presented in table 3.7 and figure 3.14.

Table 3.7: Parameters of the "testing points" validation

source	RMSE (m)	rRMSE (-)	RPD (-)	Pbias (%)
DTM	0.038	9.300	1.532	-9.9
DSM	0.046	1.424	1.482	-12.4
drone	0.082	-3.982	1.012	-7.5

In addition to this, for the DTM model, the 'test' points were ordered based on the absolute difference between the predicted value and the observed one and plotted in the catchment (figure 3.15). This does not enable us to see a particular distribution in the quality of the representation of the points.

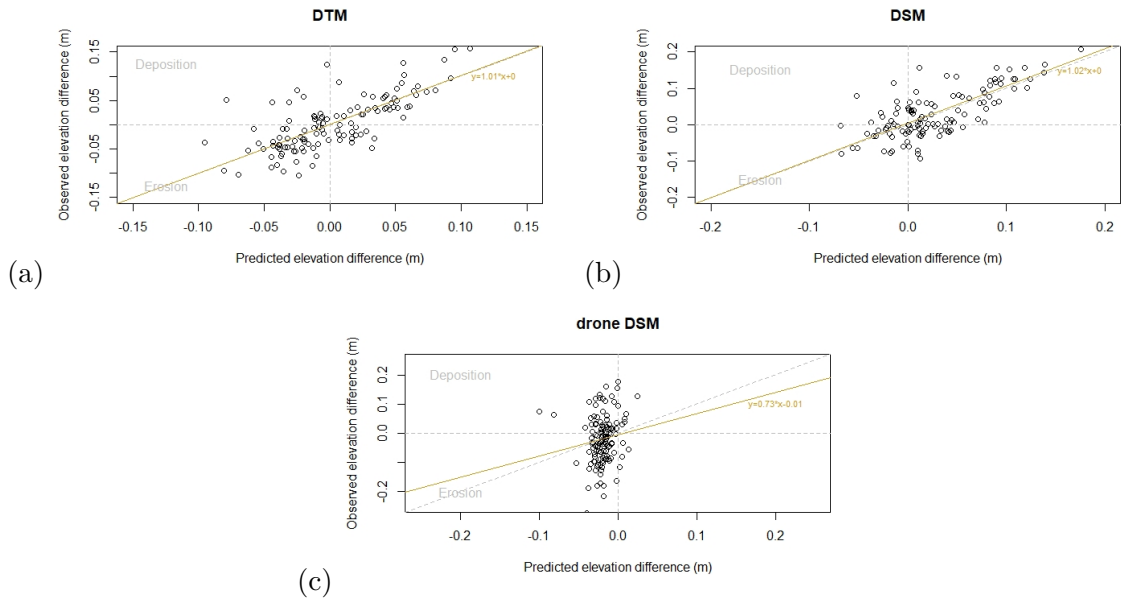

Figure 3.14: Plot of the observed values as a function of the predicted values for the 'test' dataset: (a) DTM WalOnMap, (b) DSM WalOnMap and (c) drone DSM

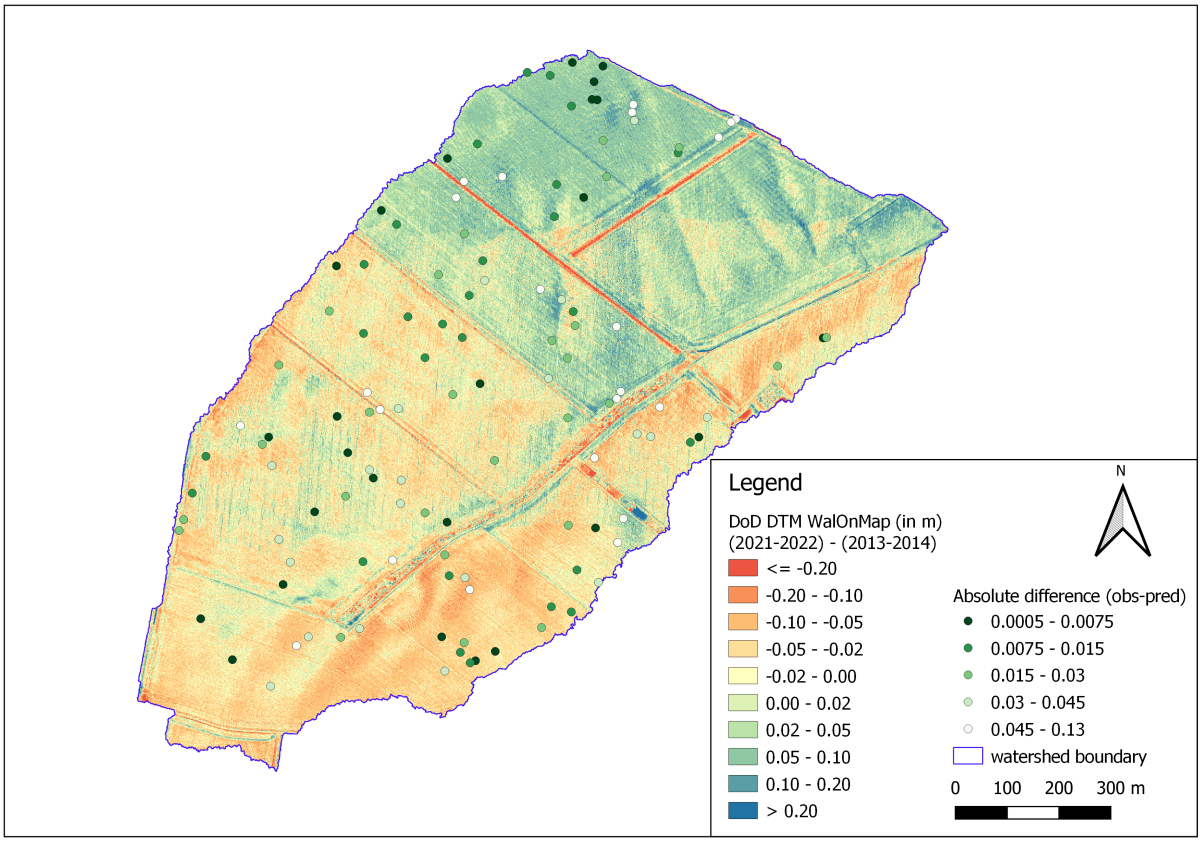

Figure 3.15: Representation of the absolute difference between observation and predictions of the test points DTM

3.3 WaTEM/SEDEM modeling

The outputs of the WaTEM/SEDEM modeling in terms of sediment production, deposition and export are presented in table 3.8.

Table 3.8: Comparison of the model outputs in WaTEM/SEDEM

section	DTM filled ?	Parcel division?	C factor	Connectivity	Total sediment production (t)	Total sediment deposition (t)	Total sediment export (t)
Connectivity & parcel division	no	yes	0.37	0	2836	2590	246
				30	2794	2554	240
				50	2766	2530	236
				70	2739	2507	233
				100	2685	2459	226
	no	no	0.37	0	2906	2709	197
				100	2901	2704	197
C factor	no	yes	map	70	2154	1970	184
Filling the DTM	fill	yes	map	70	2165	1975	181

The maps presenting water erosion, tillage erosion and total erosion are presented in figures 3.16 and 3.17.

3.3.1 Connectivity and parcel division

Since the influence of connectivity and parcel division are linked to each other, their analysis will be performed simultaneously. Indeed, if there is no parcel division, there is no need to specify a value of connectivity between the parcels, and changing the connectivity value does not influence the outputs of the model (or very slightly). When we distinguish the different parcels, we observe that the higher the connectivity, the lower the sediment production (and deposition and export). Regarding the spatial distribution of erosion and deposition, it does not influence the tillage erosion but we can see some differences in the water erosion. We can also observe that the connectivity does not influence the proportion of sediment deposition or export, which remains constant. As a reminder, in the case of the WaTEM/SEDEM model, the value of the connectivity specified *"represents to what extent water transport is stopped at the parcel border"* (see section 1.4). It means that the more we increase the value of connectivity, the more we "isolate" the field.

The reduction of sediment production due to the increase in connectivity can be explained by the fact that the more we increase the connectivity, the less water can go from one parcel to another. Since water is the agent responsible for water erosion, if there is less water flow, it results in less erosion.

3.3.2 Adapted C factor

The adaptation of the C factor to the local conditions shows a decrease in the sediment production in comparison with the default parameters. When analyzing the spatial distribution of the erosion and deposition, it can be observed that the modeled deposition remains mainly located in the rills while erosion mainly occurs in the inter-rills. We can also clearly see the sensitivity of parcel n°10, where three important erosion axes are present. This corresponds to what was observed in the fields (see section 2.1).

3.3.3 Influence of filling the DTM

Filling the DTM did not greatly influence the model outputs in this catchment. This can be explained by the fact that a function to remove the pits is already included in the WaTEM/SE-

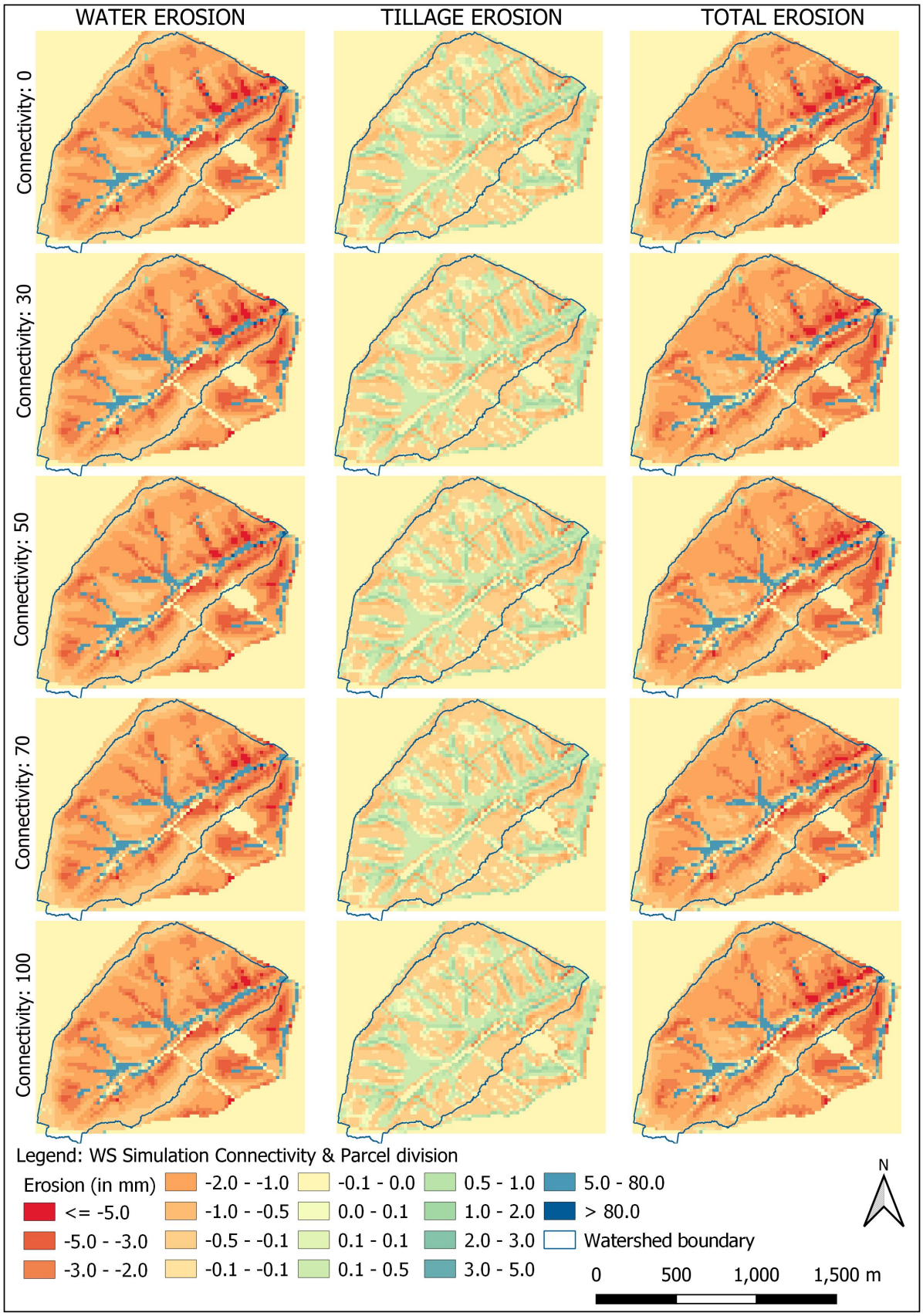

Figure 3.16: WS output maps testing influence of connectivity with parcel division

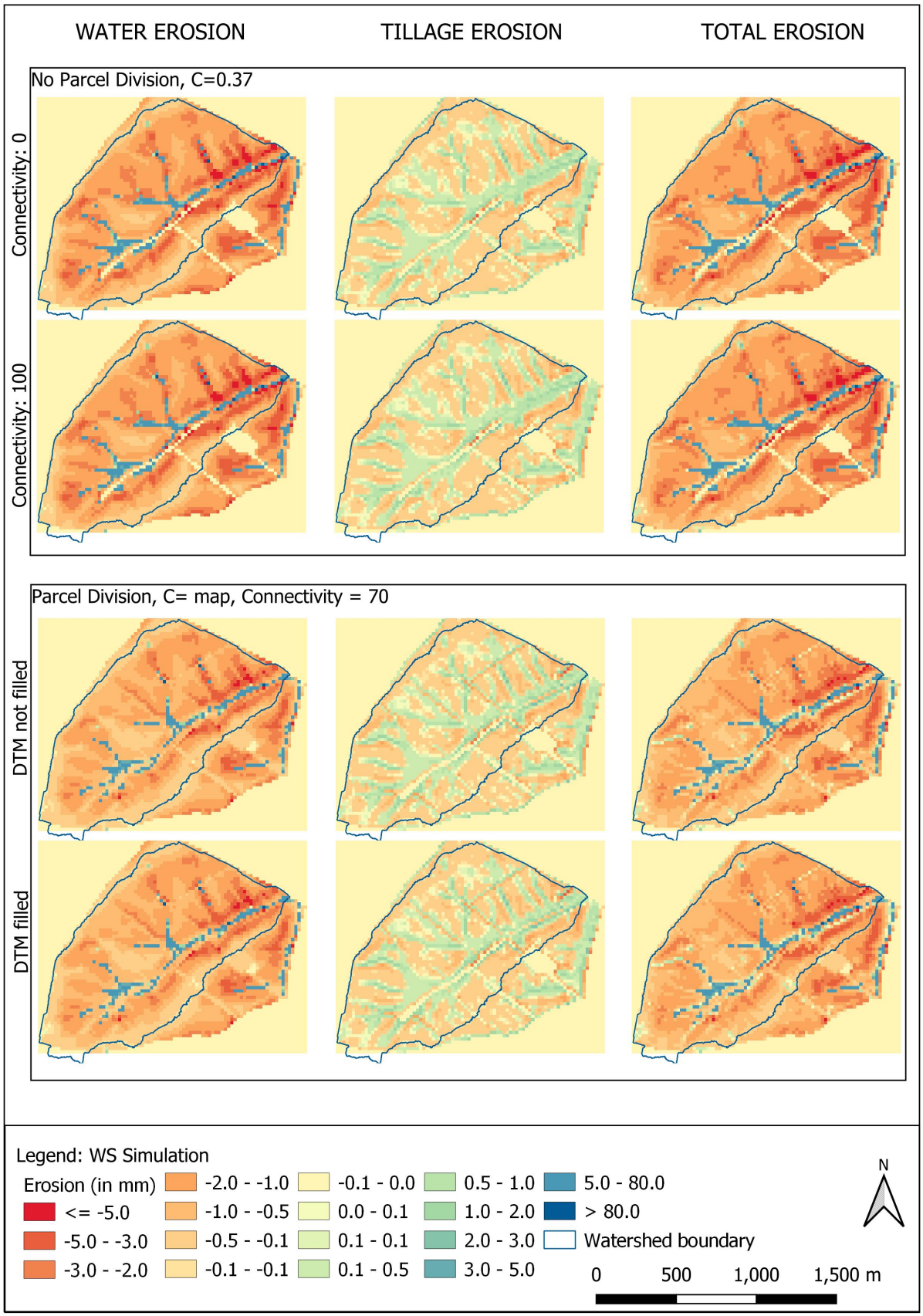

Figure 3.17: WS outputs maps testing influence of connectivity without parcel division, influence of C factor and filling DTM

DEM model. Moreover, an analysis of the pits that were removed showed that only a few pits were removed and they were relatively small.

3.4 Evolution of the streams in the catchment

The map of the different streams computed is presented in figure 3.18. Even if the accu-

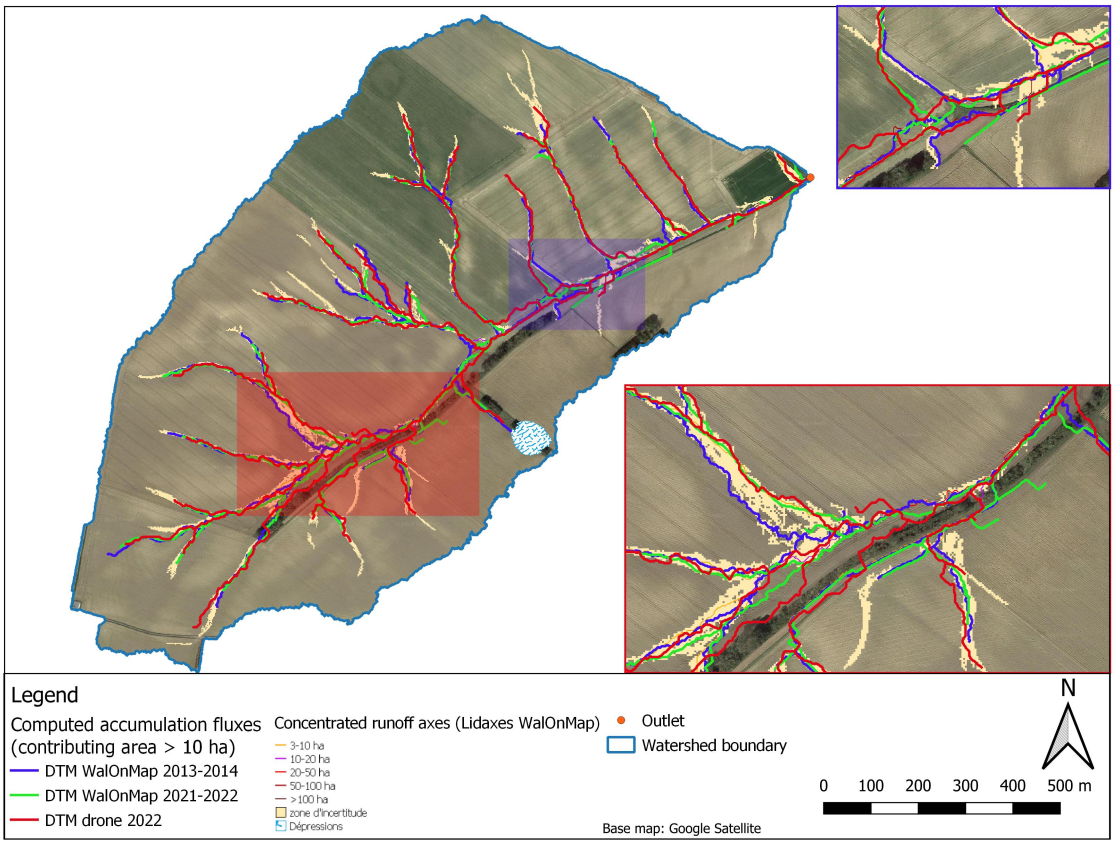

Figure 3.18: Accumulation flows computed based on different DEMs over time and Lidaxes from WalOnMap

mulation flows remain globally similar over the years, there are some differences. The lidaxes computed for 2022 with the WalOnMap and drone DTM are similar. We can also observe that the different accumulation flows stay located in the "uncertainty zone" of the WalOnMap lidaxes. This uncertainty zone corresponds in fact to the possible variations of the traces of the fluxes (WalOnMap - Géoportail de la Wallonie, 2021). It can also be noted that the real situation in the fields might be slightly different since some small channels are present between the flowmeters and sampling devices.

3.5 Comparison of the model approach and the difference of DEMs

Figure 3.19 presents a comparison of two DoD (drone and DTM Walonmap) and the WaTEM/SEDEM total erosion output, with a focus on two zones that present similarities (A and B) and differences (C) in the pattern observed in terms of erosion and deposition. As observed before, the WS outputs are characterized by deposition being mostly concentrated in the thalwegs. The aim of this comparison is to see if more deposition is also observed in the thalwegs with the DoD approach. The visual comparison reveals that we can indeed observe deposition

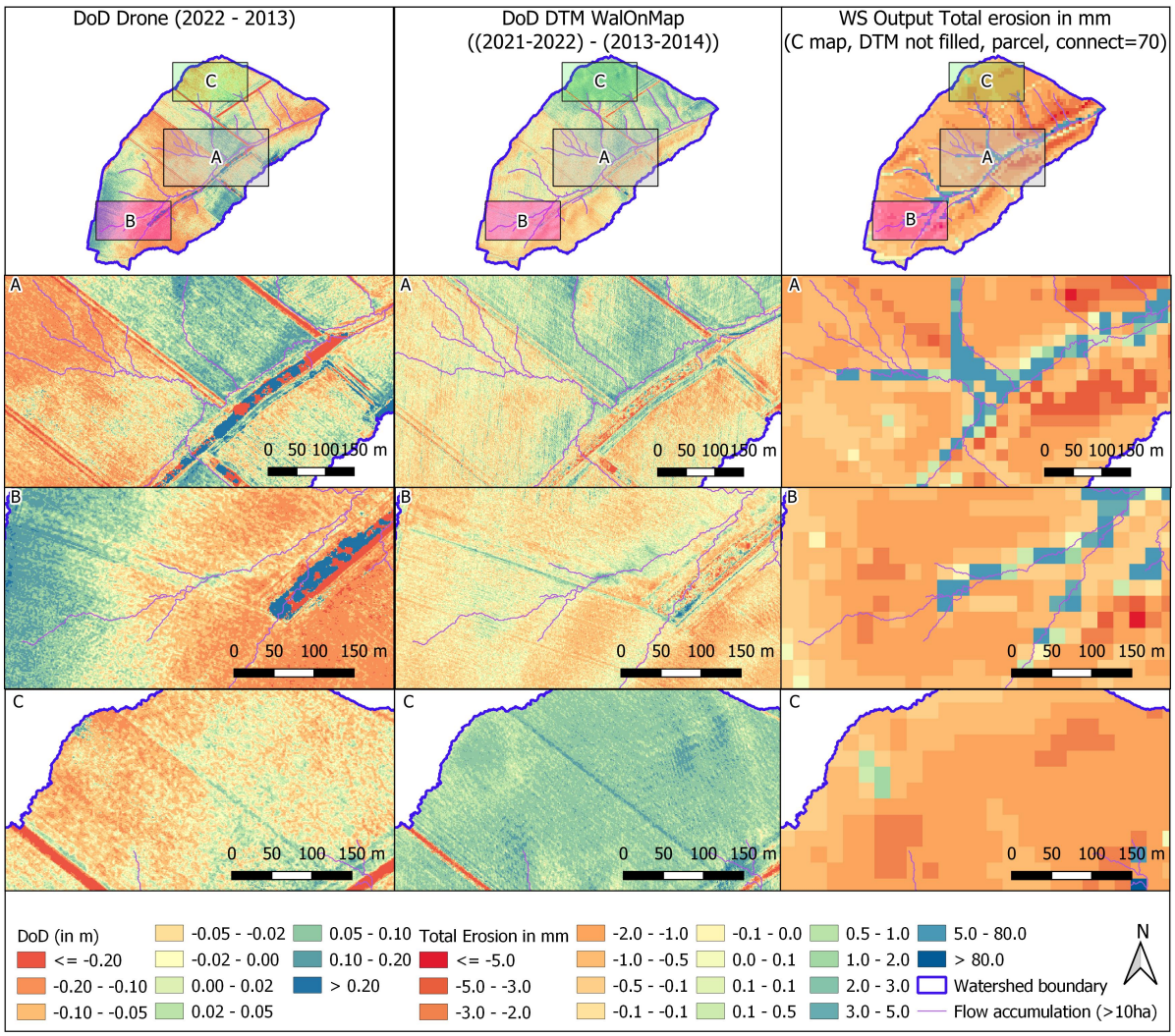

Figure 3.19: Comparison of the DoD with the model output of WaTEM/SEDEM

in the thalwegs with the DoD approach, but this remains located in specific zones (as in A and B) and is not generalized. We also observe diverging patterns like in zone C where we see mainly deposition in the DTM DoD while the WS outputs model mostly erosion and the DSM DoD shows erosion in the upper parts of the field and deposition in lower parts. In order to quantify this tendency, zonal statistics were produced for 2 different zones in the DoDs: the rills and the inter-rills (after having removed the vegetation strips). The results are shown in table 3.9. As we can see, depending on the data source of the DoD, we observe a higher (for the WalOnMap DEMs) or lower (for the drone DSMs) proportion of deposition in the rills in comparison with the inter-rills.

Table 3.9: Proportion of total deposition (in m/m^2) for rills and inter-rills and ratio (-)

Zone	**DTM**	**DSM**	**drone**
Inter-rills	0.021	0.037	0.021
Rills	0.030	0.041	0.018
Rills/inter-rills	1.4	1.1	0.9

3.6 Transects approach

The transects presented in the figure 3.20, enable to show some tendencies. The first obvious observation concerns the transitions between the parcels (lines 3 and 5). Then, we can see that some DSMs show a clear influence of crop growth (left part of line 3 drones for 2013 and 2015). The drone lines do not enable to see a clear direction in the evolution of the soil elevation. What we observe is that there are variations of about 50 cm throughout the entire period. We still observe the tendency of the drone DTM of 2022 to be lower than the rest of the data sources. This is an indication that reinforces the choice of using the DSM and not the DTM for the drone DoD, because doing so would have caused to "observe" erosion in the whole catchment. Regarding the WalOnMap lines, we do not observe this variation of 50 cm, but when focusing on some zones identified as experiencing deposition near the thalwegs (section 3.5) such as lines 1 and 6, we observe this phenomenon in the transects.

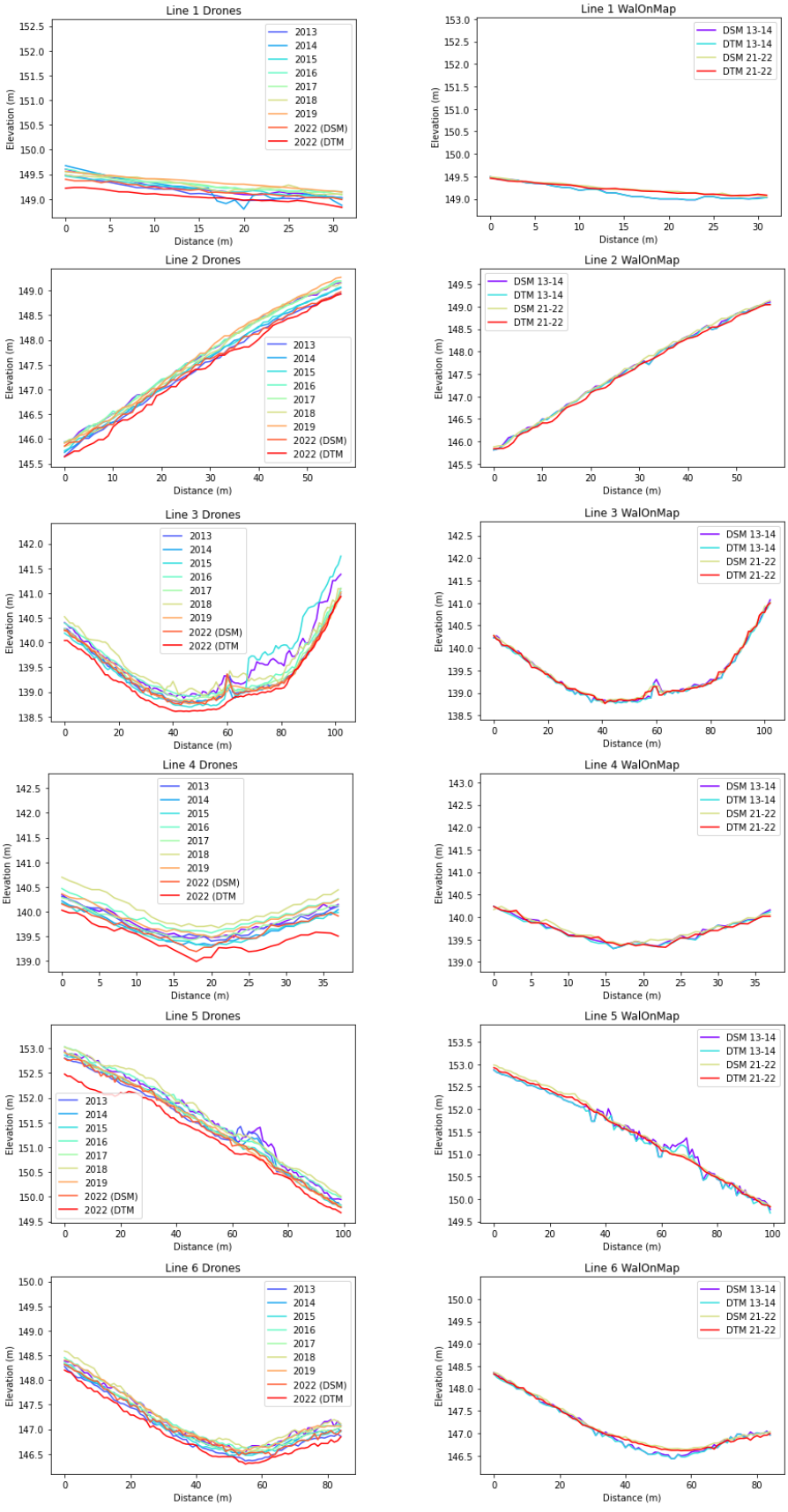

Figure 3.20: Transect lines - evolution

Chapter 4

Discussion

4.1 DEM analysis

The differences observed between the drone DoD and the WalOnMap DoDs are surprising and do not encourage full trust in those data as an actual representation of erosion and deposition. However, some interpretations are to be made.

The erosion observed in the upper parts of the catchment in the drone DoD are not in line with what is expected. Indeed, in the basic definition of erosion, sediments are expected to be transported downwards in the catchment. It could have been interesting to compute the DoD for every year to see if the temporal evolution always follows the same pattern. An investigation of the DSMs available revealed that some of them could not be used because there was either a problem in the construction of the DSM (this is the case for 2014 and 2018) or a too high influence of the vegetation (2015). Moreover, it is better to compare DSM for years in which the crop rotation is similar (Pineux et al., 2017a). The only suitable DoD that could be used is the one for 2017-2013. This DoD, presented in figure A.12 shows the same pattern as 2022-2013, which is encouraging.

The choice of using one or another type of data (drone DSMs or Lidar DTMs) is not trivial and depends on different factors. Drone DSMs have the advantage to enable fine spatial resolution (up to a few centimeters in our case) as well as better precision in z compared to WalOnMap data. However, the precision in x, y can be lower and influenced by the choice of the ground control points. The flight parameters may also influence the DSMs, with for example "border effects" due to a lower overlapping of the images near the borders of the surveyed area. The relatively low costs associated with photogrammetry enable to compute DSMs frequently. Lidar DTMs provided by WalOnMap have the advantage to cover a larger area (Wallonia) that might be useful for large-scale studies. The cost of this technology and the scale at which it is applied do not enable to compute new DEMs frequently. In conclusion, depending on the study to undertake, the most cost-effective solution should be chosen.

4.2 Statistical analysis

4.2.1 Variables

Based on the observations expressed before about the differences between the DTMs and DSMs, it could be surprising to use the DSM DoDs in the statistical analysis to try to explain erosion and deposition. Indeed, the first assumption would be that since DSMs are influenced by vegetation, they do not properly represent reality in terms of erosion and deposition when they are subtracted from each other. However, the comparison of the WalOnMAp DTM and

DSM (section 3.1.1) did not show important differences between the two data sources. Since for the drone data only DSMs could be exploited, it was decided to also use WalOnMap DSMs to enable comparison.

The choice of some variables remains based on arbitrary choices regarding the algorithms of the methods used for the computation. The computation of the C factor faced some issues related to data availability, for the input parameters needed. This was for example the case for the value of the roughness or the crop height, which were extracted from another study (Bielders et al., 2011). In order to improve the accuracy of the C factor computation of this catchment, it would be useful to monitor the soil roughness with one of the three techniques presented and used in Bielders et al. (2011). Moreover, information about the intercrops planted would be necessary (type of crop, date of sowing, and harvesting (if applicable)). However, it was noted that the data collected in the experimental catchment of Chastre were useful and already more complete than in most of the cases.

4.2.2 Outliers detection

The method chosen for the outlier detection could be improved. The method has the advantage of avoiding removing data points that could represent more extreme erosion or deposition events, that are more likely to be real and not due to precision issues in the DEMs. However, the side effect is that after the detection based on the IQR, the visual interpretation relies on an arbitrary choice of the operator. Moreover, this method would not be suitable for a larger amount of outliers to check. In order to improve this method, we could either use an algorithm that could compare the data with the surrounding pixels and determine its deviation compared to them, based on a predefined rule or more simply remove all the outliers identified with the IQR method.

4.2.3 Principal Components Analysis

The PCA revealed a positive correlation between the WalOnMap DoDs and the C factor. This means that a high deposition is associated with a high value of C. In the RUSLE equation, the opposite is true, since more erosion is associated with a high C. However, the fields that tend to be the most exposed to erosive rainfall events during critical crops periods (high C) also tend to be located more in the lower parts of the catchment (near the outlet), which also corresponds to a zone where more deposition is observed in the WalOnMap DoDs. The hypothesis here is thus that other variables influence the occurrence of deposition in those fields. This reminds us that correlation does not always mean causality.

In the same way, the negative correlation of curvature with the WalOnMap DoD could be interpreted as more erosion (negative DoD) occurring when curvature is positive, while more deposition occurs in negative curvatures. In the WS model, tillage erosion is negatively correlated with the curvature (see equation 1.7 in section 1.4), thus deposition (positive DoD) should be linked to positive curvature. In our case, curvature was computed at a 1m resolution, aiming to represent local depressions or bumps in the fields. However, we could not observe a clear pattern in the catchment (see map in the annex) and it is difficult to interpret the link between the two variables. A visual inspection of the relation between the DTM and the curvature showed that curvature seems to be positive on 'hills' and negative on the 'rills', which could explain the negative correlation between the DoD and the curvature. To improve this interpretation, it would be useful to have more insight into the algorithm used in the curvature computation (from (Zevenbergen & Thorn, 1987)) and to test other spatial resolutions. However, this correlation might be an indication that tillage erosion might play an important role in the total erosion in the catchment. A study of Van Oost et al. (2005b) conducted in another catchment in central Belgium showed that the relative importance of tillage erosion and water erosion to total soil

redistribution on agricultural land has shifted in the last decades, with a higher contribution of tillage erosion.

4.2.4 Multiple Linear Regression

The performance of the MLR is assessed by the parameters computed in the model validation. The same tendencies are observed for the different parameters depending on the data source, with a better performance of the DTM and a lower for the drone dataset. First, let us analyze the Monte-Carlo validation, which was based on the dataset used for the model construction. Over the different runs, the $RMSE$ presents a mean value of a few centimeters. The $RMSE$ is the lowest for the DTM and the highest for the drone dataset. The $rRMSE$ compares the $RMSE$ to the mean observed values. Low (absolute) values indicate good performance, meaning that the drone and DSM could perform better than the DTM. However, our data are distributed around 0, with positive and negative values, and the mean value being really close to 0. It might explain the deviation of the $rRMSE$ values compared with the other parameters. The $rRMSE$ seems to be a parameter that is not suitable for this analysis. The RPD compares the $RMSE$ to the standard deviation of the observations and represents the part of the variability in the validation dataset that is explained by the model. It means that "RPD values of 2, 3 and 4 mean that, respectively, 50%, 66.67% and 75% of the total variation in the validation dataset is caught by the model" (Meersmans et al., 2011). For the WalOnMap datasets, the model explains about 40% of the variability. For the drone dataset, the value is close to 1, meaning that the $RMSE$ is similar to the variability observed. The advantage of the $PBias$ is that it characterizes the systematic error included in the model and enables to see its direction (over - or under-estimation). It is expressed in %. The percent bias is low for the 3 datasets. The performance of the model seems to be the best for the DTM DoD, but the inspection of the boxplots presenting the variation of the parameters over the runs (figure A.8 in the appendix) shows that it is also the data source for which the variability is the highest.

This interpretation should be compared to other similar spatially distributed models from the literature. Unfortunately, most of the calibration and validation of erosion models are done on the sediment production at the outlet (Jetten et al., 2003).

Then, the analysis of the "testing points" validation shows the same tendencies, even if the values should not be compared since the approach is different. The negative values of $PBias$ reveal that there is a tendency of the model to underestimate the predictions. The plots of the observations compared to the predictions reveal that the WalOnMap datasets perform well (points aligned on the x=y function), but not the drone model. The regression equation computed between the predicted and observed points seems to be influenced by the points that are close to 0, as we would expect it to be more vertical.

The plot of the test points in the catchment based on their score on the quality of the predictions (low absolute difference between observations and predictions) did not reveal clear tendencies in the distribution of the points with the best or lowest score. It would be possible to determine if other parameters influence the quality of the prediction.

This study showed that it is possible to build a model that predicts spatially distributed erosion and deposition based on the values of the different variables and considering that erosion and deposition is assessed through the difference of DTMs approach. However, even with the encouraging validation parameters of the model, it should be noted that the erosion and deposition events remain limited in terms of range (most are limited to low values) that could be blended with the precision errors of the DTMs. More investigations are needed to verify if the performance of the model can be assessed. Nevertheless, this type of model and the variables included in it could be used to improve the determination of the transport coefficient capacity (k_{TC}) in WaTEM/SEDEM, with a spatially dependent value that varies with the variables.

4.3 Comparison of model approach and difference of DEMs

To compare the outputs of the model with the DoDs, some considerations need to be taken into account. First, the output maps of WS are expressed in mm and represent a mean annual value. In contrast, the DoDs are expressed in m and cover a period of about 10 years. Secondly, the WS outputs enable us to see the separate effects of tillage erosion and water erosion. In the DoD, we can only see the total erosion/deposition, including wind erosion and soil loss due to harvesting. Moreover, soil translocations can happen (as observed in parcel 10 after the formation of gullies), as well as soil imports resulting from crop harvesting. It could have been interesting to contact the farmers to know the quantity of soil added (or returned) to the field after tuber crops harvesting, but the contacts were hard to find and the topic remains sensitive. Anyhow, there is always a soil loss at the end of the whole process of crop harvesting. Even if soil is brought back to the field after the harvest, the amount of soil is supposed to be lower or equal to the amount of soil that is removed from the fields with the crops. Thirdly, the two maps present different resolutions, with 20m for the WS outputs and 1m for the DoDs.

However, taking all these considerations into account, it is still possible to observe similar patterns in the different approaches, especially when focusing on specific areas. We spotted deposition in the rills, as predicted with WaTEM/SEDEM, but we also observed deposition in other parts of the catchment

The statistics computed for the rills in comparison with the one of the inter-rills produce diverging results depending on the data source of the DoD. We could consider that the DTM is the most reliable because the influence of the vegetation is removed. We could then conclude that the tendency of observing more deposition in the thalwegs (rills) as it is modeled by WaTEM/SEDEM is confirmed. The results show 40% more deposition in the rills than in the inter-rills. However, we should keep in mind that the uncertainty in Z associated with the DTM is higher than the uncertainty of the drone DSM.

The WaTEM/SEDEM modeling could be improved with a calibration of the k_{TC} based on the sediment export at the outlet of the catchment (Van Rompey et al., 2001). However, for this particular study, since k_{TC} can not be spatially adapted, it would not be likely to influence in a large extent the spatial distribution of erosion and deposition, which was the main focus compared to the sediment production at the outlet.

In order to improve the comparison of the WS outputs with the DoD, an approach could be to compute successive models year after year with adapted parameters each year and sum the different outputs to determine the total erosion pattern over the whole period instead of on a mean yearly basis. However, this would require a new DTM for each year as input data. Another option could be to use the LandSoil model that computes a new DEM after each rainfall or ploughing event based on eroded and deposited soil particles (Cantreul et al., 2020).

The possibility to distinguish the different parcels based on their C value and to specify a value of connectivity between the parcels improves the representativeness of the spatial distribution of erosion and deposition. However, some other considerations could be taken into account such as the tillage direction compared to the slope direction. Moreover, the conversion of output maps from t/ha to mm is based on a bulk density of 1350 kg/m^3 uniform for the whole catchment. A more realistic option would be to consider the fact that the bulk density depends on different factors including the soil organic matter and land use and climate conditions (Robinson et al., 2022).

4.4 Transects

The variations of about 50 cm observed in the drone DSMs might be representative of the changes experienced by the agricultural soils in terms of freeze-thaw of wetting-drying cycles, or cultivation practices. Vegetation also influences the DSM as was observed in lines 3 and 5.

The WalOnMap transects enable to see deposition occurring based on a comparison of DEMs separated by a 10 years period. Line 4 was traced across one of the rills that formed on a flow axis that was observed in the fields to see if this was visible in the transects. The 2022 drone profile shows indeed a possible rill formation in the bottom of the thalweg, but it is not obvious. The analysis should be repeated to the other rills observed to see if tendencies can be extracted. The rill formation is not visible in the WalOnMap transects. The hypothesis explaining this is that the rills were filled before the 2022 Lidar survey.

The "disparition" or smoothing of the transitions between the fields observed in line 5 should not be attributed to erosion since it results from the removal of the grass strip that was located there. The differences observed in elevation are therefore likely to be due to differences in vegetation.

4.5 Future perspectives

The use of DoD to estimate erosion and deposition at a catchment level is a promising method for the future but some precautions need to be taken. A better characterization of the potential error included in the DEMs is essential. The error can be due to different steps of the analysis, like the methodology chosen for the DEM computation, and the resolution chosen. Moreover, the successive treatments applied to the DEMs such as resampling to other spatial resolutions or reprojecting to another coordinate system could also affect the final product. The evolution of the techniques also induces uncertainties, since the exact same methodology is not undertaken for all the DEM computations. In all cases, it is important to make sure that the changes observed are not due to precision differences in the measurements, especially because the erosion and deposition events are often limited to a range of a few centimeters, that may correspond to the precision in z.

More particularly, the use of DSMs requires particular attention regarding the influence that vegetation can have on the data. In order to improve the usability of those data, it would be interesting to make sure that all the flights are made on a similar date and to fully characterize the state of the catchment at this time (date of sewing, last plowing, potential recent soil addition/translocation, etc.). An option could be to focus only on a part of the catchment for which we are 100% sure that the soil was bare at the time of the flight. If the required information is not available, an option could be to use the orthophoto-plans computed with the DSMs to determine the stage of crop growth based on indices such as the Normalized Difference Vegetation Index (NDVI).

As soon as those issues will be addressed, the use of DoD or the transect approach could be an option to fill the data gap faced by scientists to calibrate and validate spatially distributed models.

In this study, the high resolution of the DSMs was not exploited since the DSMs computed at a 1m resolution were used. It could be interesting to test if the increase in the spatial resolution would improve the interpretation of the DoD or the transect approach.

The linear model built for this catchment could be improved by different means. First, more points could be taken into account in the training dataset to capture more variation. Then, other variables could be tested such as the topographic position index or a factor linking the slope

to the tillage direction. Some other options of parameters could also be tested, such as other types of curvatures, other algorithms for the LS factor, or a multi-direction flow accumulation. Moreover, we could test different spatial resolutions. In this case, regarding the small size of the catchment, the type of soil was not considered as having an important influence on erosion or deposition but an extension of this approach to larger areas could require adding the soil properties in the analysis. For example, the soil erodibility factor (K factor of the RUSLE equation) depends among others on the soil texture, organic matter content, structure and permeability (Renard et al., 1997).

Other options would be to focus on specific parts of the catchment separately, such as the upper parts, the slopes and the valleys for example. We could also analyze erosion and deposition separately.

Now that the model built for this specific catchment has shown encouraging results in terms of validation parameters, it could be used to make future predictions of erosion and deposition. Different scenarios could be possible to study, by adapting the raster layers used in the variables. For example, we could test several crop rotations or cultural practices by changing the C factor or adapting the tillage direction. It would also be interesting to test the sensitivity of the model to the variables, and especially to the C factor.

Chapter 5

Conclusion

The aim of this study was to characterize the spatial distribution of erosion and more specifically deposition in a small agricultural catchment. To do so, several approaches were investigated and compared: the difference of DEMs and the WaTEM/SEDEM model. For the DoD, different data sources were used and compared to see to what extent they could be used in assessing the spatial distribution of erosion and deposition. The WalOnMap DoDs revealed a tendency in line with the WaTEM/SEDEM model outputs, with more deposition occurring in the rills than in the inter-rills (ratio of 1.4 for the DTM). The drone DoDs, in contrast, showed a higher proportion of deposition in the inter-rills, which could be influenced by the presence of vegetation.

In addition to the DoD, a statistical analysis was conducted to determine the parameters influencing these processes. The multiple linear regression enabled to build a model that seems to predict well the erosion and deposition for the DoD computed with the WalOnMap DTM. However, a better characterization of uncertainty associated to the DTM is needed to make sure that the changes observed in terms of elevation are not due to imprecision. Several options were discussed to improve the model, including testing different spatial resolutions or different algorithms or methodologies for some variables such as LS, tillage direction, or curvature. The type of model and the variables tested in this study could be used to improve spatially distributed models such as WaTEM/SEDEM.

The drone DSMs, if computed on a bare soil can enable to see tendencies in erosion and deposition with the DoD approach. The transects approach revealed that DSM computed each year enabled to see a variation in the elevation, but this analysis was not able to extract clear observation of erosion or deposition in specific features. A more in-depth and systematic analysis could be done to determine if patterns can be seen. This could be performed on a higher resolution to see to what extent it influences the analysis.

For the WalOnMap DTMs, the transect approach enable spot deposition in the thalwegs, which was in line with the WaTEM/SEDEM model outputs.

In conclusion, even if some developments are still required in terms of uncertainty associated with DEMs, they seem to be a promising approach for improving the knowledge about the spatial distribution of erosion and deposition. The DoD as well as the transects approach can be useful methods to study this process on a 10-year interval.

Bibliography

Batista, P. V., Davies, J., Silva, M. L., & Quinton, J. N. (2019). On the evaluation of soil erosion models: Are we doing enough ? *Earth-Science Reviews*, 197(102898). https://doi.org/10.1016/j.earscirev.2019.102898

Bielders, C., Maugnard, A., Feltz, N., Cordonnier, H., Degré, A., Destain, M., & Colard, F. (2011). *Convention GISER-Convention de recherche d'intérêt général gestion intégrée sol érosion ruissellement.*

Borselli, L., Cassi, P., & Torri, D. (2008). Prolegomena to sediment and flow connectivity in the landscape: A GIS and field numerical assessment. *Catena*, 75, 268–277. https://doi.org/10.1016/j.catena.2008.07.006

Cantreul, V., Bielders, C., Calsamiglia, A., & Degré, A. (2018). How pixel size affects a sediment connectivity index in central belgium. *Earth Surface Processes and Landforms*, 43, 884–893. https://doi.org/10.1002/esp.4295

Cantreul, V., Pineux, N., Swerts, G., Bielders, C., & Degré, A. (2020). Performance of the LandSoil expert-based model to map erosion and sedimentation: application to a cultivated catchment in central Belgium. *Earth Surface Processes and Landforms*, 45, 1376–1391. https://doi.org/10.1002/esp.4808

Cerdan, O., Souchère, V., Lecompte, V., Couturier, A., & Le Bissonnais, Y. (2001). Incorporating soil surface crusting processes in an expert-based runoff model:Sealing and Transfer by Runoff and Erosion related to Agricultural Management. *Catena*, 46, 189–205. https://doi.org/10.1016/S0341-8162(01)00166-7

Dautrebande, S., Cordonnier, H., Thirion, M., & Bielders, C. (2006). Lutter contre l'érosion des terres. *Les livrets de l'agriculture*, 12.

European Commission (2015). *Good Agricultural and Environmental Conditions (GAEC).* https://marswiki.jrc.ec.europa.eu/wikicap/index.php/Good_Agricultural_and_Environmental_Conditions_(GAEC). Accessed 09/05/2023.

European Commission (n.d.). *The common agricultural policy: 2023-27.* https://agriculture.ec.europa.eu/common-agricultural-policy/cap-overview/cap-2023-27_en. Accessed 09/05/2023.

Gobeyn, S., De Vleeschouwer, N., Renders, D., Vand de Wauw, J., Van Hoey, S., & Gert Verstraeten, G. (2021a). *R-factor.* https://cn-ws.github.io/rfactor/index.html.

Gobeyn, S., Van de Wauw, J., De Vleeschouwer, N., Renders, D., Van Ransbeeck, N., Verstraeten, G., & Deproost, P. (2021b). Herziening van de neerslagerosiviteitsfactor R voor de Vlaamse erosiemodellering.

Hudson, N. W. (1993). *Field Measurement of Soil Erosion and Runoff*, volume 68 of *FAO Soils Bulletin*. Food and Agriculture Organization of the United Nations. https://books.google.be/books?id=rS1fiFU3rOwC

IRM (2020). *Rapport climatique 2020 de l'information aux services climatiques, Institut Royal Météorologique*. https://www.meteo.be/resources/misc/climate_report/RapportClimatique-2020.pdf.

Jetten, V., Govers, G., & Hessel, R. (2003). Erosion models: quality of spatial predictions. *Hydrological Processes*, 17(5), 887–900. https://doi.org/10.1002/hyp.1168

Lisein, J., Pineux, N., Pierrot-Deseilligny, M., Degré, A., & Lejeune, P. (2017). Détection de l'érosion dans un bassin versant agricole par comparaison d'images multidates acquises par drone. *Revue Française de Photogrammétrie et de Télédétection*, 213, 133–141. https://doi.org/10.52638/rfpt.2017.196

Loba, A., Waroszewski, J., Tikhomirov, D., Calitri, F., Christl, M., Sykuła, M., & Egli, M. (2021). Tracing erosion rates in loess landscape of the Trzebnica Hills (Poland) over time using fallout and cosmogenic nuclides. *Journal of Soils and Sediments*, 21(8), 2952–2968. https://doi.org/10.1007/s11368-021-02996-x

Maugnard, A., Van Languenakers, P., Bielders, C., & Degré, A. (2022). Cartographie du risque de dégradation des sols et de transfert des pollutions agricoles diffuses au cours d'eau - Lot 1 : Mise à jour des données.

Meersmans, J., van Wesemael, B., Goidts, E., van Molle, M., De Baets, S., & De Ridder, F. (2011). Spatial analysis of soil organic carbon evolution in belgian croplands and grasslands, 1960–2006. *Global Change Biology*, 17, 466–479. https://doi.org/10.1111/j.1365-2486.2010.02183.x

Morgan, R. (2005). *Soil Erosion and Conservation* (3rd ed.). Blackwell Publishing.

Notebaert, B., Vaes, B., Verstraeten, G., & Govers, G. (2006). *WaTEM/SEDEM version 2006 Manual*.

Parsons, A. J. (2019). How reliable are our methods for estimating soil erosion by water? *Science of the Total Environment*, 676, 215–221. https://doi.org/10.1016/j.scitotenv.2019.04.307

Pineux, N., Lisein, J., Swerts, G., Bielders, C., Lejeune, P., Colinet, G., & Degré, A. (2017a). Can dem time series produced by uav be used to quantify diffuse erosion in an agricultural watershed? *Geomorphology*, 280, 122–136. https://doi.org/10.1016/j.geomorph.2016.12.003

Pineux, N., Michel, B., Legrain, X., Bielders, C., Degré, A., & Colinet, G. (2017b). Diachronic soil surveys: A method for quantifying long-term diffuse erosion? *Geoderma Regional*, 10, 102–114. https://doi.org/10.1016/j.geodrs.2017.06.001

Renard, K., Foster, G., Weesies, G., McCool, D., & Yoder, D. (1997). *Predicting Soil Erosion by Water: A Guide to Conservation Planning With the Revised Universal Soil Loss Equation (RUSLE)*, volume 703. U.S. Department of Agriculture.

Robinson, D., Thomas, A., Reinsch, S., Lebron, I., Feeney, C., Maskell, L., Wood, C., Seaton, F., Emmett, B., & Cosby, B. (2022). Analytical modelling of soil porosity and bulk density across the soil organic matter and land-use continuum. *Scientific reports*, 12(1), 7085. https://doi.org/10.1038/s41598-022-11099-7

Rotili, L. (2023). *Politique agricole commune: les agriculteurs inquiets à cause d'une mesure sur l'érosion des sols - RTBF.be*. https://www.rtbf.be/article/politique-agricole-commune-les-agriculteurs-inquiets-a-cause-dune-mesure-sur-lerosion-des-sols-11170933. Accessed 09/05/2023.

SPW (2023). *PAC 2023-27 et érosion des sols - Portail de l'agriculture wallonne.* http://agriculture.wallonie.be/cms/render/live/fr/sites/agriculture/home/ruralite/protection-des-sols/prevention-et-lutte-contre-l-erosion-des-sols/pac-erosion.html. Accessed 29/03/2023.

Stolte, J., Tesfai, M., Øygarden, L., Kværnø, S., Keizer, J., Verheijen, F., Panagos, P., Ballabio, C., & Hessel, R., editors (2016). *Soil threats in Europe.* https://doi.org/10.2788/488054(print);10.2788/828742(online). EUR 27607 EN

Van Oost, K., Govers, G., Cerdan, O., Thauré, D., Rompaey, A. V., Steegen, A., Nachtergaele, J., Takken, I., & Poesen, J. (2005a). Spatially distributed data for erosion model calibration and validation: The Ganspoel and Kinderveld datasets. *Catena*, 61, 105–121. https://doi.org/10.1016/j.catena.2005.03.001

Van Oost, K., Govers, G., & Desmet, P. (2000). Evaluating the effects of changes in landscape structure on soil erosion by water and tillage. *Landscape Ecology*, 15, 577–589. https://doi.org/10.1023/A:1008198215674

Van Oost, K., Van Muysen, W., Govers, G., Deckers, J., & Quine, T. (2005b). From cater to tillage erosion dominated landform evolution. *Geomorphology*, 72, 193–203. https://doi.org/10.1016/j.geomorph.2005.05.010

Van Rompey, A. J., Verstraeten, G., Van Oost, K., Govers, G., & Poesen, J. (2001). Modelling mean annual sediment yield using a distributed approach. *Earth Surface Processes and Landforms*, 26, 1221–1236. https://doi.org/10.1002/esp.275

Verheijen, F., Jones, R., Rickson, R., & Smith, C. (2009). Tolerable versus actual soil erosion rates in europe. *Earth-Science Reviews*, 94, 23–28. https://doi.org/10.1016/j.earscirev.2009.02.003

Walling, D. & Quine, T. (1992). The use of caesium-137 measurements in soil erosion surveys. *Erosion and sediment monitoring programmes in river basins. Proc. international symposium, Oslo, 1992, IAHS*, 210, 143–152.

WalOnMap - Géoportail de la Wallonie (2021). *Fiche descriptive: Lidaxes (version 2) - axes de concentration du ruissellement et données associées - série.* https://geoportail.wallonie.be/catalogue/43c57664-9548-4dd0-93fd-696f5bf85537.html. Accessed 31/05/2023.

Williams, R. D. (2012). DEMs of Difference. *Geomorphological Techniques.*

Wischmeier, W. & Smith, D. (1978). Predicting rainfall erosion losses: a guide to conservation planning. *Agriculture Handbook*, 537.

Zevenbergen, L. W. & Thorn, C. R. (1987). Quantitative analysis of land surface topography. *Earth Surface Processes and Landforms*, 12, 47–56. https://doi.org/10.1002/esp.3290120107

Zhidkin, A., Gennadiev, A., Fomicheva, D., Shamshurina, E., & Golosov, V. (2023). Soil erosion models verification in a small catchment for different time windows with changing cropland boundary. *Geoderma*, 430(116322). https://doi.org/10.1016/j.geoderma.2022.116322

Appendix A

Additional figures

This appendix contains figures providing additional details to complement the discussion in chapters 3 and 4.

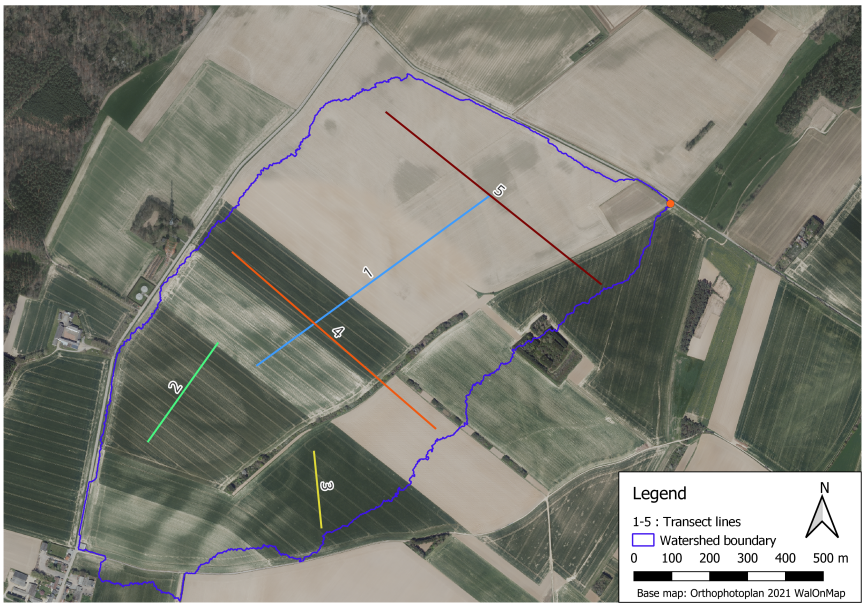

Figure A.1: Transect lines to compare the DEMs data sources

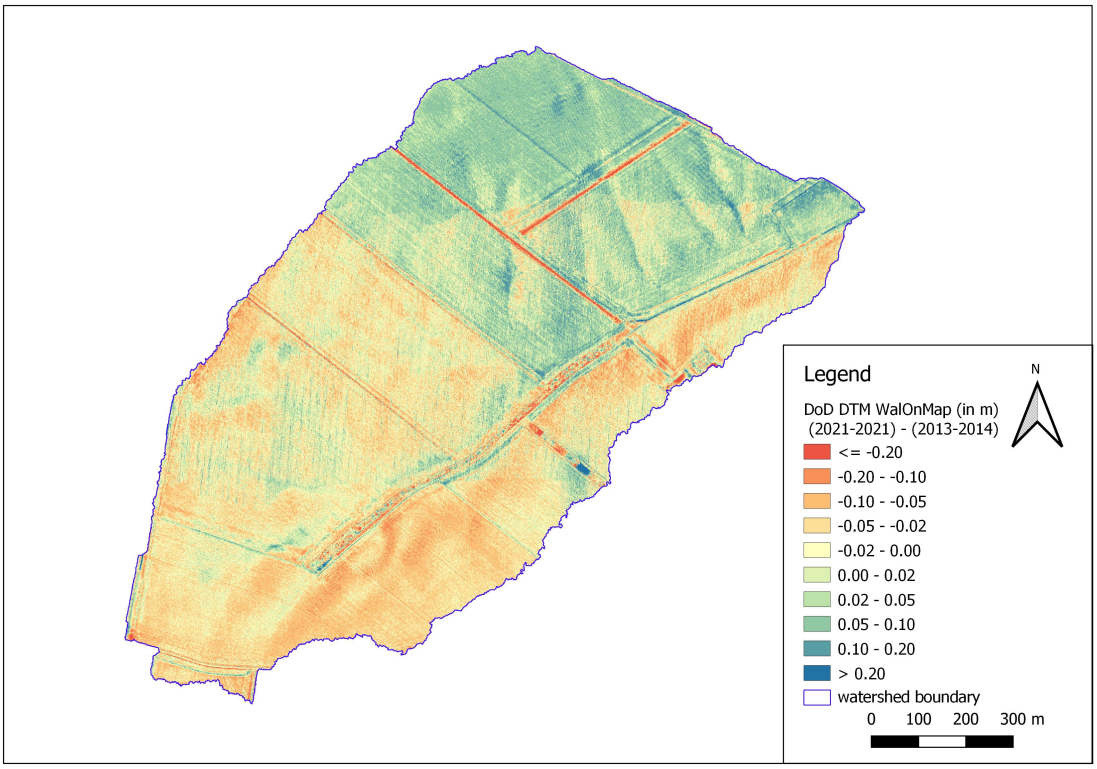

Figure A.2: DoD DTM WalOnMap

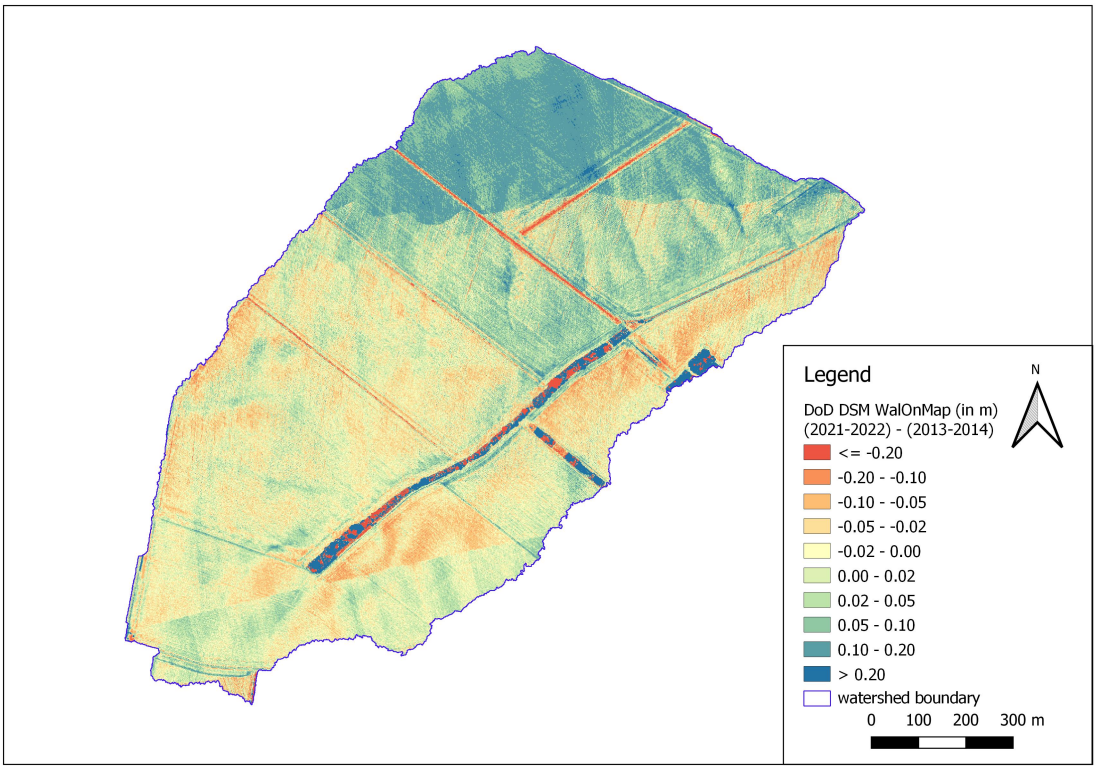

Figure A.3: DoD DSM WalOnMap

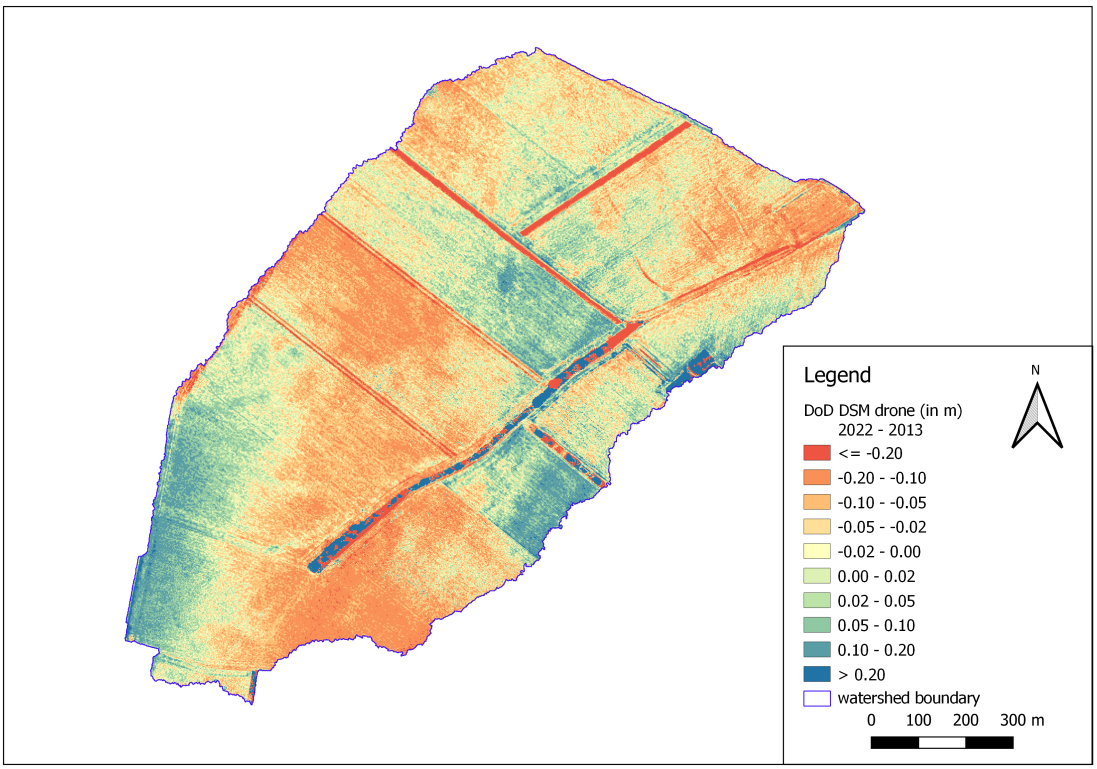

Figure A.4: DoD DSM drone 2022-2013

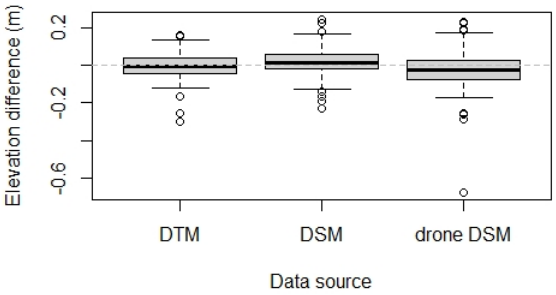

Figure A.5: Boxplot of DoD points

(a)

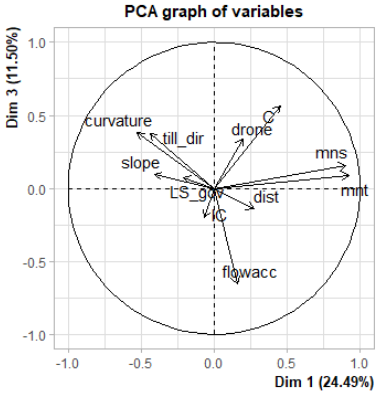

(b)

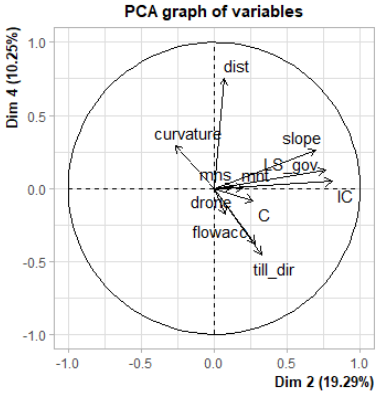

(c)

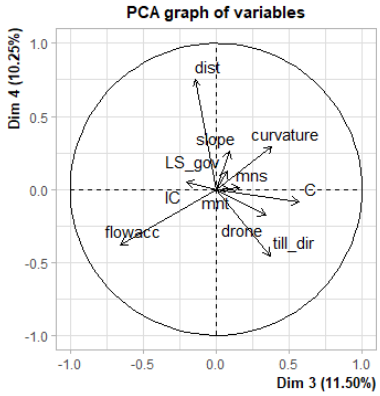

Figure A.6: Circles of correlation of the PCA

(a)

```
$Dim.1
$quanti
           correlation       p.value
mnt          0.9216956 1.766152e-176
mns          0.9041460 1.069842e-158
C            0.4518938  7.917501e-23
dist         0.2727819  1.049715e-08
drone        0.1942431  5.440335e-05
flowacc      0.1564858  1.193939e-03
LS_gov      -0.2080211  1.502438e-05
slope       -0.4073054  1.868941e-18
till_dir    -0.4412831  9.969556e-22
curvature   -0.5275129  6.896537e-32
```

(b)

```
$Dim.2
$quanti
           correlation       p.value
IC           0.8125237 1.987987e-101
LS_gov       0.7632594  1.859752e-82
slope        0.6974266  2.484576e-63
till_dir     0.3239876  7.226950e-12
flowacc      0.2816917  3.274432e-09
C            0.2655747  2.613324e-08
mnt          0.1987782  3.596420e-05
mns          0.1297474  7.330803e-03
curvature   -0.2659151  2.504646e-08
```

(c)

```
$Dim.3
$quanti
           correlation       p.value
C            0.5673309 1.178010e-37
curvature    0.3828269 2.560432e-16
till_dir     0.3746845 1.203293e-15
drone        0.3403382 5.178475e-13
mns          0.1583358 1.041315e-03
dist        -0.1420049 3.311525e-03
IC          -0.2009879 2.929563e-05
flowacc     -0.6574013 4.592926e-54
```

(d)

```
$Dim.4
$quanti
           correlation       p.value
dist         0.7532884 3.559266e-79
curvature    0.2908031 9.525278e-10
slope        0.2611822 4.496966e-08
LS_gov       0.1221338 1.164052e-02
drone       -0.1795324 1.953705e-04
flowacc     -0.3792197 5.109388e-16
till_dir    -0.4537320 5.058879e-23
```

Figure A.7: PCA: significant correlations of the variables on the main axes

(a) (b)

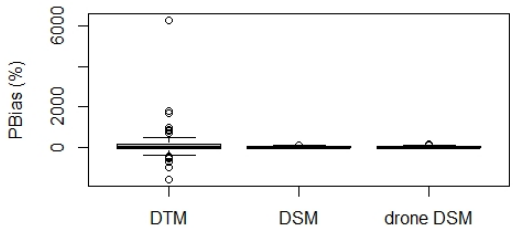

(c)

Figure A.8: Boxplots of the parameters of the Monte Carlo validation

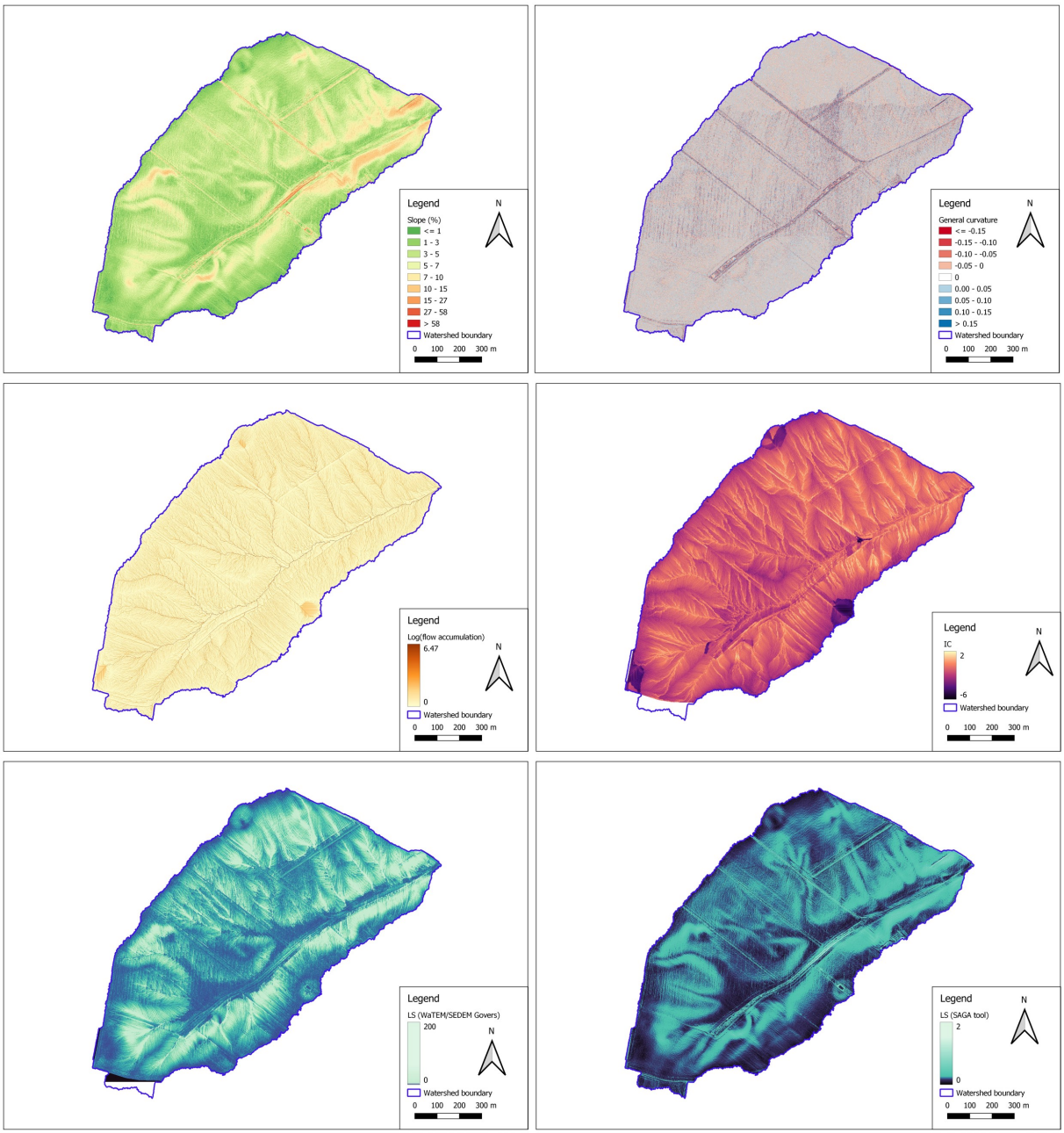

Figure A.9: Variables of statistical analysis (1)

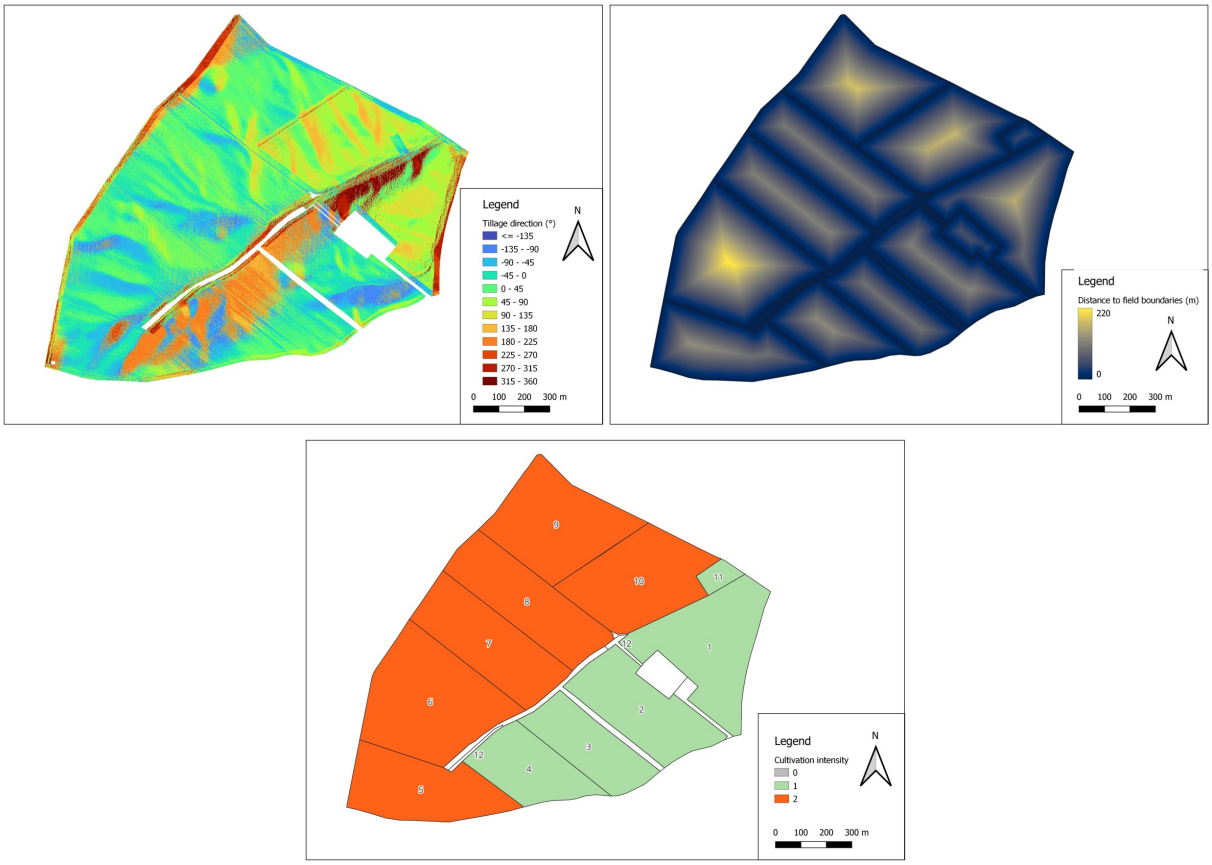

Figure A.10: Variables of statistical analysis (2)

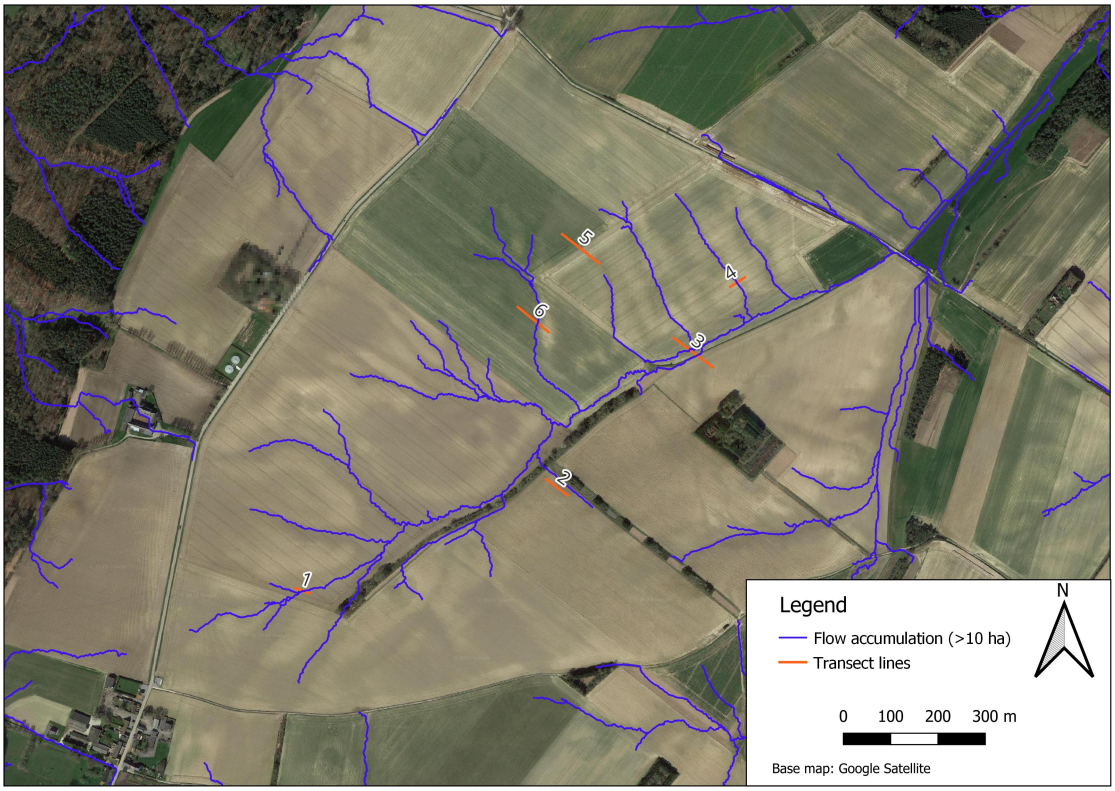

Figure A.11: Location of transect lines in the catchment

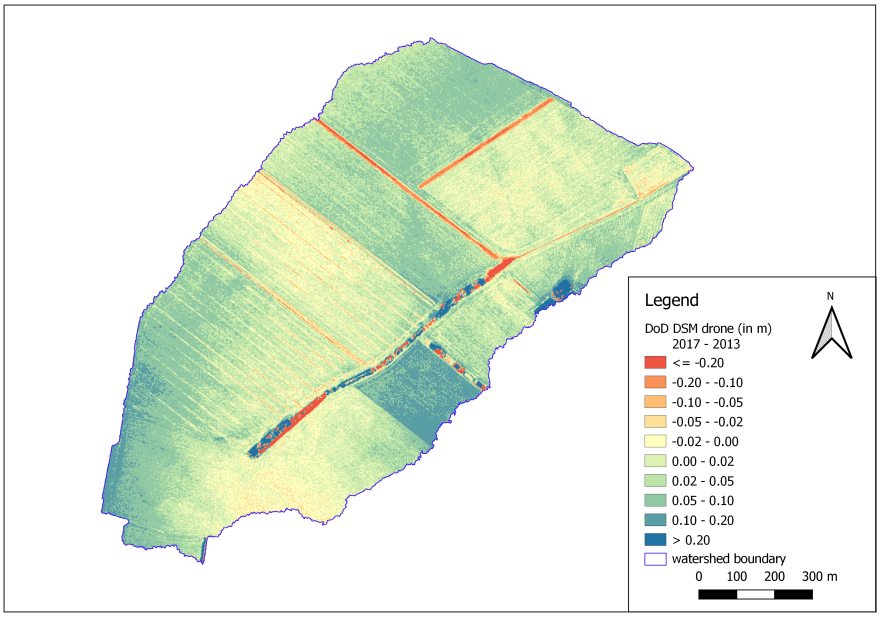

Figure A.12: DoD DSM drone 2017-2013